1987

Determination of thermodynamic and kinetic properties of concanavalin A and various sugars using high-performance affinity chromatography

Robert Michael Moore
Iowa State University

INFORMATION TO USERS

While the most advanced technology has been used to photograph and reproduce this manuscript, the quality of the reproduction is heavily dependent upon the quality of the material submitted. For example:

- Manuscript pages may have indistinct print. In such cases, the best available copy has been filmed.
- Manuscripts may not always be complete. In such cases, a note will indicate that it is not possible to obtain missing pages.
- Copyrighted material may have been removed from the manuscript. In such cases, a note will indicate the deletion.

Oversize materials (e.g., maps, drawings, and charts) are photographed by sectioning the original, beginning at the upper left-hand corner and continuing from left to right in equal sections with small overlaps. Each oversize page is also filmed as one exposure and is available, for an additional charge, as a standard 35mm slide or as a 17"x 23" black and white photographic print.

Most photographs reproduce acceptably on positive microfilm or microfiche but lack the clarity on xerographic copies made from the microfilm. For an additional charge, 35mm slides of 6"x 9" black and white photographic prints are available for any photographs or illustrations that cannot be reproduced satisfactorily by xerography.

Moore, Robert Michael

DETERMINATION OF THERMODYNAMIC AND KINETIC PROPERTIES OF CONCANAVALIN A AND VARIOUS SUGARS USING HIGH-PERFORMANCE AFFINITY CHROMATOGRAPHY

Iowa State University PH.D. 1987

PLEASE NOTE:

In all cases this material has been filmed in the best possible way from the available copy. Problems encountered with this document have been identified here with a check mark __✓__.

1. Glossy photographs or pages _____
2. Colored illustrations, paper or print _____
3. Photographs with dark background _____
4. Illustrations are poor copy _____
5. Pages with black marks, not original copy _____
6. Print shows through as there is text on both sides of page _____
7. Indistinct, broken or small print on several pages ✓
8. Print exceeds margin requirements _____
9. Tightly bound copy with print lost in spine _____
10. Computer printout pages with indistinct print _____
11. Page(s) _____ lacking when material received, and not available from school or author.
12. Page(s) _____ seem to be missing in numbering only as text follows.
13. Two pages numbered _____. Text follows.
14. Curling and wrinkled pages _____
15. Dissertation contains pages with print at a slant, filmed as received ✓
16. Other _____

_____

_____

University
Microfilms
International

Determination of thermodynamic and kinetic properties of concanavalin A and various sugars using high-performance affinity chromatography

by

Robert Michael Moore

A Dissertation Submitted to the
Graduate Faculty in Partial Fulfillment of the
Requirements for the Degree of
DOCTOR OF PHILOSOPHY

Department: Chemistry
Major: Analytical Chemistry

Approved:

Signature was redacted for privacy.

In Charge of Major Work

Signature was redacted for privacy.

For the Major Department

Signature was redacted for privacy.

For the Graduate College

Iowa State University
Ames, Iowa

1987

TABLE OF CONTENTS

GENERAL INTRODUCTION

Background

Affinity chromatography can be used to determine the equilibrium and rate constants for specifically interacting biological complexes. The first report of affinity chromatography being used for this type of measurement was by Andrews et al. (1), who determined the equilibrium constants for the binding of D-glucose and N-acetyl-D-glucosamine to the enzyme A protein of human lactose synthetase. The enzyme was injected onto a column containing α-lactalbumin immobilized on a Sepharose matrix, with the mobile phase containing D-glucose or N-acetyl-D-glucosamine. Equations were derived relating the retention volume of the eluted enzyme with the concentration of the sugar in the mobile phase. Dunn and Chaiken (2) expanded this model to include the interaction of the immobilized ligand and the analyte. Using the derived relations, the equilibrium constants were determined for the binding of staphylococcal nuclease to thymidine-5'-phosphate-3'-aminophenylphosphate-Sepharose and thymidine-3',5'-bis-phosphate, which was present in the mobile phase. It was in this study that the phrase "quantitative affinity chromatography" was first applied to the determination of equilibrium constants by affinity chromatography. The equilibrium constants of many biochemical systems have been determined using this technique, as reviewed by Chaiken (3) and Dunn (4).

Fewer studies have been undertaken to determine rate constants using affinity chromatography. Several different experimental designs have been

used. The most widely used method has been based on the broadening of a band of solute during an isocratic elution with a competitive inhibitor present in the mobile phase, as suggested by Denizot and Delaage (5). Long and Chaiken (6) used this technique to determine the kinetics of the interaction of ribonuclease and uridine-5'-(Sepharose-4-aminophenyl-phosphate)- 2'(3')phosphate. The results indicated that while the ratio of the dissociation rate constant to the association rate constant agreed with the equilibrium constant measured for the complex in solution, each rate constant was several orders of magnitude lower than the rate constant for the interaction in solution. The shortcomings of soft gels were demonstrated by Katoh et al. (7), who demonstrated that the rate-limiting step for several interactions was the mass transfer in the stagnant mobile phase.

With the development of high performance affinity chromatography using small, rigid supports with much better mass transfer characteristics, the determination of rate constants was again investigated (8-11). The rate constants that have been measured in these studies have been one or more orders of magnitude lower than the values determined in free solution. It has been suggested by Anderson and Walters (11) that these low values are due to inadequacies in the band-broadening theories and/or the dominance of mass transport kinetics over adsorption/desorption kinetics.

An alternative approach, based on frontal chromatography, has been proposed by Chase (12). In this work, relationships between the slope and position of the breakthrough curve and the equilibrium and kinetic constants were derived. These relations were tested against experimental data from an immobilized monoclonal antibody - β-galactosidase system. Comparison

between immobilized ligand-analyte rate constants to solution rate constants is not possible because this method has not yet been applied to a complex whose kinetic parameters are known.

A third method for the determination of association rate constants was suggested by Sportsman et al. (13), who observed that not all of the insulin injected onto a column containing immobilized antisera would bind. Hage et al. (14) expanded on this observation, developed a model for the behavior and tested the model with experimental data from the immobilized protein A - immunoglobulin G system. Called the split-peak method, it has not yet been applied to a complex whose kinetic parameters are known. Data will be presented in this dissertation that applies this method to a complex whose solution rate constants are known, the concanavalin A - 4-methylumbelliferyl α-D-mannopyranoside complex.

Another method for the measurement of dissociation rate constants has been proposed by Moore and Walters (15). This method, called the peak-decay method, is based on the ability to cause an analyte molecule to undergo a single dissociation from an immobilized ligand during passage through a column by manipulating the mobile phase. This dissertation will present data that establishes the conditions required for the immobilized concanavalin A - 4-methylumbelliferyl α-D-manno-pyranoside complex. Dissociation rate constants were measured over a range of temperatures and the energy of activation calculated. Dissociation constants were also measured for the immobilized concanavalin A - p-nitrophenyl α-D-mannopyranoside complex and the immobilized concanavalin A - ovalbumin complex.

Determination of Equilibrium Constants

The retention in affinity chromatography can be described by the equilibrium constants of the various species that are in the chromatographic system. For an affinity chromatographic system in which the ligand L is immobilized and a solute E is isocratically eluted using a competing inhibitor I, the reactions of interest and their equilibium constants are:

$$E + L \rightleftarrows EL \qquad K_3 = \frac{\{EL\}}{[E]\{L\}} \qquad (1)$$

$$I + L \rightleftarrows IL \qquad K_2 = \frac{\{IL\}}{[I]\{L\}} \qquad (2)$$

The accolades represent a surface concentration (mol/dm^2). The mass balance of the ligand is given by Equation 3:

$$m_L = A(\{L\} + \{EL\} + \{IL\}) \qquad (3)$$

where m_L is the total moles of ligand in the column and A is the surface area of the packing material in the column (dm^2). From the definition of capacity factor (k') one can write:

$$k' = \frac{A\{EL\}}{V_m[E]} \tag{4}$$

where V_m is the void volume (L). Substitution of Equations 1-3 into Equation 4 yields:

$$k' = \frac{K_3 m_L}{V_m(1 + K_2[I])} \tag{5}$$

Expressions similar to Equation 5 can be obtained from the work of Dunn and Chaiken (2), Eilat and Chaiken (16) and Hethcote and DeLisi (17). Taking the reciprocal of Equation 5 produces:

$$\frac{1}{k'} = \frac{V_m}{K_3 m_L} + \frac{V_m K_2[I]}{K_3 m_L} \tag{6}$$

The equilibrium constants K_2 and K_3 can thus be determined from the slope and intercept of a plot of $1/k'$ versus [I]. This equation can also be derived for "normal-role" affinity chromatography, in which the inhibitor interacts with the solute.

The effect of temperature on the capacity factor can be determined by considering the effect a change in temperature has on each term in Equation

5. While V_m and [I] will be changed slightly, the major effect will result from changes in K_2 and K_3. By measuring k' at various temperatures and inhibitor concentrations, the reaction enthalpies and entropies can easily be determined from Equations 6 and 7:

$$\ln K_{eq} = \frac{-\Delta H^\circ}{RT} + \frac{\Delta S^\circ}{R} \qquad (7)$$

In this manner, the thermodynamics of both the ligand-analyte and ligand-inhibitor can be studied.

Determination of Rate Constants by Split-Peak Method

The evaluation of rate constants is based on the theoretical work of Giddings and Eyring, who stated that there is a probability e^{-kt} (where k is the first-order rate constant and t is the column void time) that a molecule will not adsorb as it passes through the column (18). Although Giddings and Eyring (18) and Sportsman et al. (13) considered only the adsorption step to be rate-limiting, it could be that the diffusion through the stagnant mobile phase is rate-limiting. These processes are modelled by Hethcote and DeLisi (17) and described by the equations:

$$E_e \rightleftarrows E_p \qquad K_1 = \frac{k_1}{k_{-1}} = \frac{V_p}{V_e} \tag{8}$$

$$E_p + L \rightleftarrows E\text{-}L \qquad K_3 = \frac{k_3}{k_{-3}} = \frac{\{E\text{-}L\}}{[E]\{L\}} \tag{9}$$

The symbol E represents the solute present in the flowing mobile phase (or excluded volume, e), the stagnant mobile phase (or pore volume, p) or bound to the immobilized ligand (L). The diffusional rate constants (k_1,k_{-1}) are related to the excluded volume (V_e) and pore volume accessible to the solute (V_p). Equation 9 describes the binding between the solute and the immobilized ligand. If K_3 is large enough to provide irreversible binding, the possible transfers between the three states for the solute simpilfy to:

$$E_e \rightleftarrows E_p \rightarrow E\text{-}L \tag{10}$$

Let p(x,t), q(x,t) and r(x,t) be probability densities for a solute molecule to be at position x at time t, in the mobile phase outside the pores, in the mobile phase inside the pores and bound to the immobilized ligands, respectively, in a column with length h. By using a conservation of mass approach, the following system of differential equations can be obtained (14):

$$\frac{\partial p}{\partial t} = u_e \frac{\partial p}{\partial x} - k_1 p + k_{-1} q \tag{11}$$

$$\frac{\partial q}{\partial t} = k_1 p - k_{-1} q - k_3(L) q \tag{12}$$

$$\frac{\partial r}{\partial t} = k_3(L) q \tag{13}$$

in which u_e is the linear velocity of an excluded, nonretained solute and the other terms are as defined earlier.

The initial layer containing solute molecules at the top of the column is assumed to be sufficiently small so that it can be considered to be an instantaneous source given by a Dirac delta function. Thus, the initial conditions for $0 \leq x \leq h$ are:

$$p(x,0) = \delta(x-h),\ q(x,0) = 0,\ r(x,0) = 0 \tag{14}$$

Since there are no molecules at the top of the bed when the initial layer leaves, the boundary conditions for $t > 0$ are:

$$p(h,t) = q(h,t) = r(h,t) = 0 \tag{15}$$

If we integrate Equations 11-13 from 0 to infinity with respect to t and use the initial conditions given in Equation 15, we obtain:

$$r(x,\infty) = k_3[L]\int_0^\infty q(x,t)\,dt = k_1\int_0^\infty p(x,t)\,dt - k_{-1}\int_0^\infty q(x,t)\,dt \tag{16}$$

$$\int_0^\infty q(x,t)\,dt = \frac{k_1}{k_{-1} + k_3[L]}\int_0^\infty p(x,t)\,dt \tag{17}$$

$$u_e\frac{\partial}{\partial x}\int_0^\infty p(x,t)\,dt = -\delta(x-h) - r(x,\infty) =$$

$$-\delta(x-h) - \frac{k_1}{1 + k_{-1}/k_3[L]}\int_0^\infty p(x,t)\,dt \tag{18}$$

Letting $y = h - x$, we use Laplace transforms to solve Equation 18 with the boundary conditions given in Equation 15 to obtain:

$$\int_0^\infty u_e p(x,t)\,dt = e^{-c(h-x)} \tag{19}$$

$$r(x,\infty) = ce^{-c(h-x)} \tag{20}$$

where

$$c = \frac{k_1/u_e}{1 + k_{-1}/k_3[L]} \tag{21}$$

Note that $u_e p(0,t)$ is the elution profile and $r(x,\infty)$ is the distribution of retained molecules in the column. Thus, the fractions of total molecules that are free (f) and bound (b) are:

$$f = \int_0^\infty u_e p(0,t)\, dt = e^{-ch} \tag{22}$$

$$b = \int_0^\infty r(x,\infty)\, dx = 1 - e^{-ch} \tag{23}$$

Combining Equations 21 and 22 yields:

$$\frac{-1}{\ln f} = \frac{u_e}{h}\left[\frac{1}{k_1} + \frac{k_{-1}}{k_1 k_3[L]}\right] \tag{24}$$

The volumetric flow rate (F) is defined as:

$$F = \frac{u_e V_e}{h} \tag{25}$$

Combining Equations 8, 24 and 25 gives:

$$\frac{-1}{\ln f} = F\left[\frac{1}{k_1 V_e} + \frac{1}{k_3 m_L}\right] \tag{26}$$

From Equation 26, it can be seen that a plot of the negative inverse of the natural logarithm of the fractional area for a nonretained peak vs. the volumetric flow rate will be a straight line with an intercept of zero. If diffusion is rate-limiting, the slope will equal $1/k_1 V_e$. If adsorption is rate-limiting, the slope will equal $1/k_3 m_L$. The slope would take on an intermediate value if the two processes occurred at the same rate.

Two criteria must be met before Equation 26 can be applied: the values of f and b must be independent of sample size (i.e., linear elution conditions) and the adsorption must be essentially irreversible on the time scale of the experiment (i.e., large k' and/or small k_{-3}). Although the derivation specifies a Dirac delta function as the sample input, this is not a necessary requirement. Sample that is applied in a plug injection can be regarded as a series of delta functions, in each of which a fraction f elutes without binding.

Adsorption kinetics are more likely to be rate limiting when m_L is small. This is related not only to column length, but also to column surface area and

ligand density. An affinity chromatograhic column often contains 10- to 1000- fold fewer ligand sites than an ion-exchange or reversed-phase column, so split peaks are more likely to occur in affinity chromatographic systems. However, if the flow rate is increased, every column should exhibit split-peak behavior at some point.

When split-peak behavior is desired in order to measure adsorption kinetics, the number of ligand sites and column size are often minimized. While this does increase the probability that split-peak behavior will be observed, it should be remembered that reducing the number of ligand sites also reduces the capacity factor, as shown in Equation 5. If the dissociation rate constant is of the proper magnitude, a careful balance must be reached in providing the correct number of ligand sites to produce the split-peak behavior and still maintain a large enough capacity factor to insure the validity of Equation 26.

Determination of Rate Constants by Peak-Decay Method

The theory for the peak-decay method is also based on the model utilized by Hethcote and DeLisi (17) for isocratic affinity chromatography. This model is modified such that the adsorption sites are first saturated with solute (by means of a frontal rather than zonal application of E), then the column is washed to remove any solute not bound to the ligand. A high concentration of competing inhibitor is next applied to the column in a frontal mode so that the retention of the solute is suddenly reduced nearly to zero. The solute is then eluted under isocratic conditions. Since the

inhibitor does not itself cause dissociation of the immobilized ligand-solute complex, but instead functions to prevent readsorption by filling any empty adsorption sites, the value of the dissociation rate constant is not altered.

The elution profile of the solute leaving the column cannot, in general, be easily used to extract kinetic data. However, if extreme conditions are utilized, useful information may be obtained. In particular, if readsorption and diffusion back into the stagnant mobile phase are prevented, then only a single dissociation will take place for each immobilized ligand-solute complex. Then the elution profile should resemble an exponential decay with a rate constant equal to the dissociation rate or the diffusion rate, whichever is smaller.

Mathematically, the peak-decay method is described by the reactions:

$$E\text{-}L \xrightarrow{k_{-3}} E_p + L \tag{27}$$

$$E_p \xrightarrow{k_{-1}} E_e \tag{28}$$

which are just the irreversible equivalents of the equilibria in Equations 8 and 9. To prevent reversibility completely requires infinitely large competing inhibitor concentrations (so that $k' = 0$) and a column of zero length (so that diffusion back into the stagnant mobile phase is prevented). Under such conditions, the differential equations describing reactions 27 and 28 are as follows:

$$\frac{dm_{E-L}}{dt} = - k_{-3} m_{E-L} \tag{29}$$

$$\frac{dm_{Ep}}{dt} = k_{-3} m_{E-L} - k_{-1} m_{Ep} \tag{30}$$

where m is the number of moles of solute. Assuming that all of the solute is initially adsorbed and of the total amount m_{E_0}, and that $k_{-3} < k_{-1}$, the equations can be solved (19) in terms of the amount eluted up to time t:

$$m_{Ee} = \frac{m_{E_0}}{k_{-1} - k_{-3}} [k_{-1}(1 - e^{-k_{-3}t}) - k_{-3}(1 - e^{-k_{-1}t})] \tag{31}$$

The elution profile is the derivative of Equation 31:

$$\frac{dm_{Ee}}{dt} = \frac{k_{-1} k_{-3} m_{E_0}}{k_{-1} - k_{-3}} (e^{-k_{-3}t} - e^{-k_{-1}t}) \tag{32}$$

If $k_{-3} << k_{-1}$, then Equation 32 reduces to a simple exponential decay. The rate constant k_{-3} is obtained from the slope of a plot of the natural logarithm of the elution profile:

$$\ln \frac{dm_{Ee}}{dt} = \ln(m_{E_0} k_{-3}) - k_{-3} t \qquad (33)$$

.An analogous derivation can be made for the case where $k_{-1} < k_{-3}$.

The use of a finite inhibitor concentration and column length will result in some readsorption of the solute onto the stationary phase and some diffusion of solute back into the stagnant mobile phase. This will cause further band-broadening, a shallower elution profile, and an apparent low value for the rate constant determined from the slope of the logarithm of the profile. However, it is possible to find useful conditions under which Equation 33 provides a reasonably accurate description of the elution profile. These conditions are most easily obtained by means of compute simulations.

Computer Simulation of Chromatographic Processes

The computer model used to simulate both the split-peak and peak decay processes is based on the first-order reactions equivalent to Equations 8 and 9:

$$E_e \underset{k_{-1}}{\overset{k_1}{\rightleftarrows}} E_p \underset{k_{-3}}{\overset{k_3^*}{\rightleftarrows}} E\text{-}L \qquad (34)$$

The first-order adsorption rate constant is defined:

$$k_3^* = \frac{k_3 m_L}{V_p} \tag{35}$$

The general solution to this reaction was derived by Rakowski (20) and can easily be recast in terms of capacity factor, pore volume and excluded volume.

To utilize Equation 34 for column chromatography, the convective mass transport of the solute in the excluded volume must also be taken into account. This can be done by dividing an imaginary column longitudinally into a large number of slices and radially into three regions (flowing and stagnant mobile phase, and stationary phase). Each iteration of the computer consists of equilibrating the solute contained within one slice between the three radial regions according to the solution of Equation 34, then moving the solute in the excluded volume into the excluded volume of the next slice (the excluded linear velocity, u_e, is one slice per iteration). The solute leaving the last slice is monitored.

The time between recalculation of the amounts of solute in each slice and phase is one iteration. If the rate constants are approximately one iteration^{-1} or larger, the system is close to equilibrium and the elution profile can be predicted from the Craig distribution (21). This undesirable characteristic can be avoided by using smaller values for the rate constants ($\lesssim 0.1$ iteration^{-1}). By decreasing the rate constants and proportionally

increasing the number of slices of column length, one can easily ensure that the results have converged to a single value. This model was previously used for isocratic studies (11).

When used to simulate split-peak conditions, the number of slices that the solute must pass through before it leaves the column is reduced, thus reducing the amount of time the solute spends in the column. As the residence time in the column is decreased, split-peak behavior is observed. Other conditions are similar to those in the isocratic studies.

For use in the peak-decay studies, the program is modified so that solute is initially distributed throughout the column. At time zero, a plug of mobile phase containing inhibitor begins to move down the column, the capacity factor decreases to some predetermined value behind the mobile-phase front, and the solute begins to undergo dissociation, readsorption and diffusion, just as in the isocratic method.

The simulation does not take into account broadening and dilution of the competing inhibitor front, nor does it take into account the finite number of ligand sites. Inclusion of the former process in the model would probably cause the elution profile to be broader, while the latter would cause it to be narrower.

EXPERIMENTAL DETAILS

Reagents

Concanavalin A, type IV (Con A), 4-methylumbelliferyl α-D-mannopyranoside (MUM), 4-methylumbelliferyl α-D-galactopyranoside (MUGA), p-nitrophenyl α-D-mannopyranoside (PNPM), methyl α-D-mannopyranoside, type II (MDM) and ovalbumin, type VI (OVA) were purchased from Sigma (St. Louis, MO). γ-Glycidoxypropyltrimethoxysilane was obtained from Petrarch (Bristol, PA). Hypersil WP-300, 5-μm particle diameter, was purchased from Alltech (Deerfield, IL). Sodium cyanoborohydride, 1,1'-carbonyldiimidazole and mannose were purchased from Aldrich (Milwaukee, WI).

Con A was further purified according to the procedure of Cunningham et al. (22), with two exceptions: dialysis of the Con A supernatant was against the mobile phase sodium acetate buffer described below rather than water and no lyophilization was done. Dioxane was stored over molecular sieves. All other compounds were reagent grade and used as recieved.

Apparatus

A Model 334 liquid chromatograph (Beckman, Berkeley, CA) was modified by replacing the mixing chamber with a tee. A Model V^4 variable-wavelength absorbance detector (ISCO, Lincoln, NE) with a 1-μL flowcell was used for the isocratic and the split-peak studies at a wavelength of 316 nm for MUM and 306 nm for PNPM. For the peak-decay studies, a Model 757 variable-

wavelength absorbance detector (Kratos, Ramsey, NJ) with a 12-µL flowcell was used for detection at 316 nm for MUM and MUGA, 306 nm for PNPM and 280 nm for OVA. An Apple IIe computer (Cupertino, CA) with an Interactive Microware interface (State College, PA) was used for data acquisition. A refrigerated circulating bath (Fisher, St. Louis, MO) was used to maintain the temperature of the column and the mobile phase.

The columns used were variations of the "minicolumn" designed by Walters (23), with the outer connector modified as a water jacket. Stainless steel columns with dimensions of 49.7 mm x 4.1 mm I.D. and 6.3 mm x 2.1 mm I.D. were used for isocratic and peak-decay studies, respectively. Teflon columns with dimensions of 4.7 mm x 0.79 mm I.D. were used for split-peak studies. In these columns, 2-µm screens (Alltech) were used in place of frits.

A 100-W ultrasonic cleaner (Fisher) and a wrist-action shaker (Burrell, Pittsburgh, PA) were used for the stationary phase preparation. A Haskel air-driven pump (Alltech) and a Model 705 stirred-slurry column packer (Micromeritics, Norcross, GA) were used for packing the column for the isocratic studies. A Beckman Model 112 pump was used for packing columns for the split-peak studies.

Stationary Phase Preparation

Diol-bonded Hypersil WP-300 was prepared according to a published aqueous silanization procedure (24). Two methods were used to immobilize the Con A on the support.

Schiff base method (25).

A mixture of 0.8 g diol-bonded silica and 40 mL of 5 mg/mL HIO_4 in 80% acetic acid was degassed by sonication under vacuum for 15 min, then shaken for 30 min at room temperature. The product was filtered onto a fine-porosity glass filter, washed with methanol and sucked dry. The solid was resuspended in a volume of 25 mL of a solution containing 9.8 mg/mL purified Con A in 0.50 M sodium acetate buffer (pH 5.00), containing 1.0 mM calcium chloride and 1.0 mM manganese chloride. The reaction mixture also included 160 mg of sodium cyanoborohydride to reduce the Schiff base. The mixture was degassed as above and shaken at 4 °C for 6 days. The immobilized Con A concentration was found to be 39 mg/g silica as the result of the bicinchoninic protein assay (Pierce, Rockford, IL). This stationary phase was packed into a 49.7 mm x 4.10 mm I.D. column using the upward-flow stirred-slurry system or into a 6.3mm x 2.1 mm I.D. column using the vacuum-slurry method.

CDI Method (26).

A mixture of 0.1 g diol-bonded silica, 25 mg CDI and 3 mL dry dioxane was degassed as above, then shaken for 30 min at room temperature. The product was filtered onto a fine-porosity glass filter, washed with dry dioxane and sucked dry. The solid was resuspended in 2 mL of purified Con A solution described above, degassed and shaken at 4 °C for 7 days. The immobilized Con A concentration was found to be 38 mg/g silica as the

result of the bicinchoninic protein assay. This stationary phase was packed in a 6.3 mm x 2.1 mm I.D. column using the vacuum-slurry method.

A high-coverage packing material was prepared as above with two exceptions: 5 mL of the Con A solution was used and 1 mL of 0.206 M mannose was added to protect the Con A binding sites. The Con A concentration was found to be 115 mg/g silica. This stationary phase was packed in a 4.7 mm x 0.79 mm I.D. column using a downward-flow slurry method.

The number of active ligand sites for all columns were determined by breakthrough analysis using MUM as the solute. To estimate the effect of non-specific binding on m_L (11), three concentrations of MUM were used. Comparison of the breakthrough data with the protein assay suggest all of the Con A immobilized was active and available to the MUM.

Chromatographic Conditions

The mobile phase for the split-peak studies was the buffer described above. For the determination of equilibrium constants, the mobile phase was a solution of mannose of varying concentration in the buffer. The weak mobile phase for the peak-decay studies was the buffer described above. The strong mobile phase used for the Con A - sugar studies was 0.1 M mannose in the buffer. The strong mobile phase for the Con A - OVA studies contained 1.5 M MDM. The step change from application to elution buffer caused a shift

in the baseline. However, baseline correction using a blank run was unnecessary because the baseline disturbance did not overlap with the tail of the peak.

The volumetric flow-rates were calibrated by gravimetry. Column void time (t_m) was determined by the injection of sodium nitrate. A non-specific retention time (t_{ns}) was determined using MUGA as the eluite. Where appropriate, the non-specific retention was subtracted from the measured retention times. Representative data is summarized in Table 1.

Statistical moments for the isocratic studies were determined from the peak-center-at-half-height using a Gaussian approximation. The slope of the natural logarithm of the tailing portion of the peak-decay data was calculated using the method of Guggenheim (27). The peak obtained from the immobilized Con A - OVA complex was smoothed using a cubic polynomial after the method of Savitisky and Golay (28) before the computation of the slope.

Table 1. Column parameters

Column dimensions mm	Immobilization method	V_m µL	m_L nmol
49.7 × 4.1	EA	410	610[a] 650[b] 720[c] 650[d]
6.3 × 2.1	EA	12	1.5[b] 1.3[d]
	CDI	12	1.4[b] 1.3[d]
4.7 × 0.79	CDI	1.5[e]	0.18[b] 0.18[d]

[a]Determined from breakthrough analysis using MUM concentration of 6.12 µM.
[b]Determined from breakthrough analysis using MUM concentration of 9.25 µM.
[c]Determined from breakthrough analysis using MUM concentration of 25.1 µM.
[d]Determined from protein assay and experimental packing densities.
[e]Calculated value.

RESULTS AND DISCUSSION

Determination of Equilibrium Constants by Zonal Analysis

Equilibrium constants in the temperature range of 4° to 30° C for the solute MUM and the inhibitor mannose were determined from plots of the reciprocal of the capacity factor vs. inhibitor concentration using Equation 6. The plots (Figure 1) exhibited excellent linearity. The results are listed in Table 2. Comparing the equilibrium constant at 25° C for MUM to reported values for the dimeric Con A - MUM complex in solution (29) shows a 1.4-fold difference, but the values obtained are in excellent agreement with values of the immobilized system as determined by Anderson and Walters (11). This difference between homogeneous and heterogeneous systems may be due to the effects of changing from solution concentrations to surface concentrations and/or due to conformational changes in the Con A as a result of immobilization. It is interesting to note that the immobilizied dimer value is nearer to tetrameric solution values than dimeric values. The loss of steric freedom on immobilization would be similar to that lost when a tetrameric unit is formed from dimers. This would make the tetramer a better system to compare the immobilized Con A to than dimeric Con A. Other equilibrium constants measured by affinity chromatography have typically been within a factor of two of solution data (2,3).

The reaction enthalpies and entropies for MUM and mannose were calculated by plotting the equilibrium constants from Table 2 using Equation 7 (Figure 2). In addition, these reaction parameters for MUM were determined

Figure 1. Plots used to determine equilibrium constants. Column dimensions: 49.7 × 4.1 mm. Flow rate: 1.00 mL/min. (△) 4°C, (▲) 10°C, (▫) 15°C, (■) 20°C, (◇) 25°C, (◆) 30°C

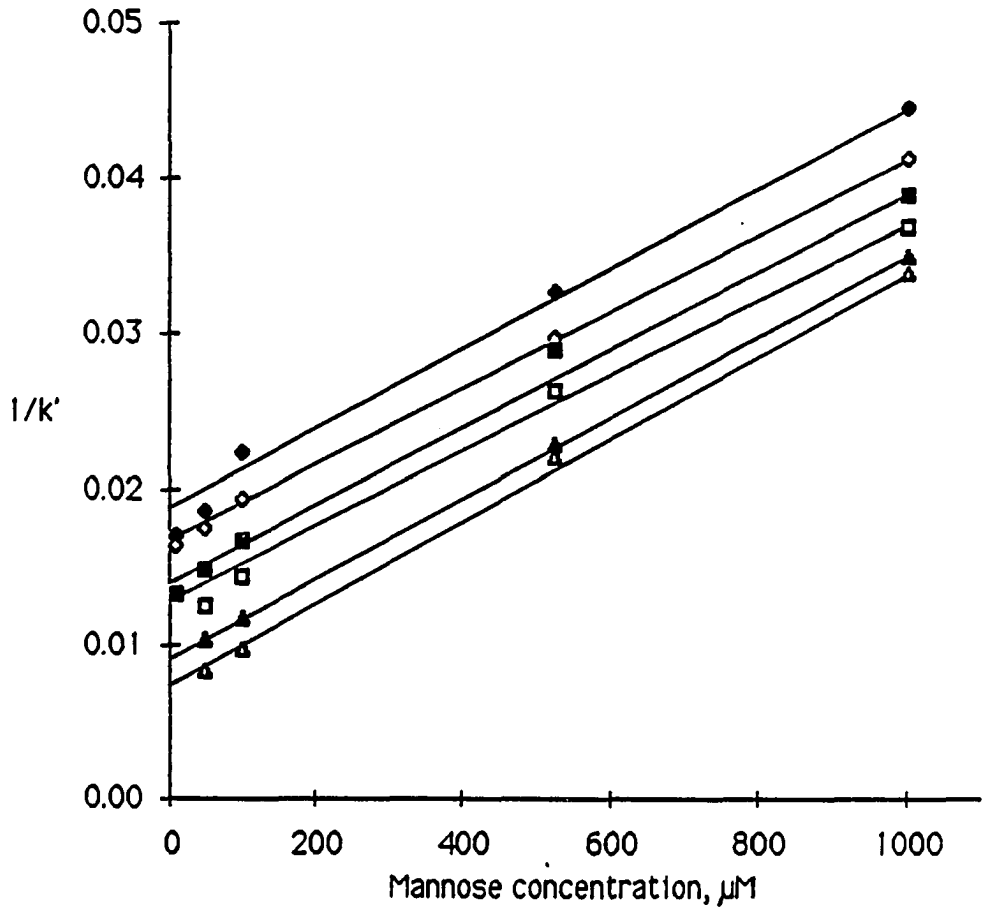
0.05
0.04
0.03
0.02
0.01
0.00
1/k'
0
200
400
600
800
1000
Mannose concentration, µM

Table 2. Equilibrium Constants for MUM and Mannose

Temperature °C	K_{eq}, mannose $M^{-1}x10^{-3}$	K_{eq}, MUM $M^{-1}x10^{-4}$			
4	3.84	10.4			
10	2.83	8.10			
15	2.19	6.28			
20	1.87	5.34			
25	1.52	4.50	3.36[a]	4.26[b]	4.5[c]
30	1.41	3.41			

[a]Reference 29, dimeric Con A.
[b]Reference 29, tetrameric Con A.
[c]Reference 11, immobilized Con A.

Figure 2. Plots used to determine binding enthalpies and entropies.
Figure a displays data for MUM (♦) and mannose (◇), Figure b for MUGA.

(a)

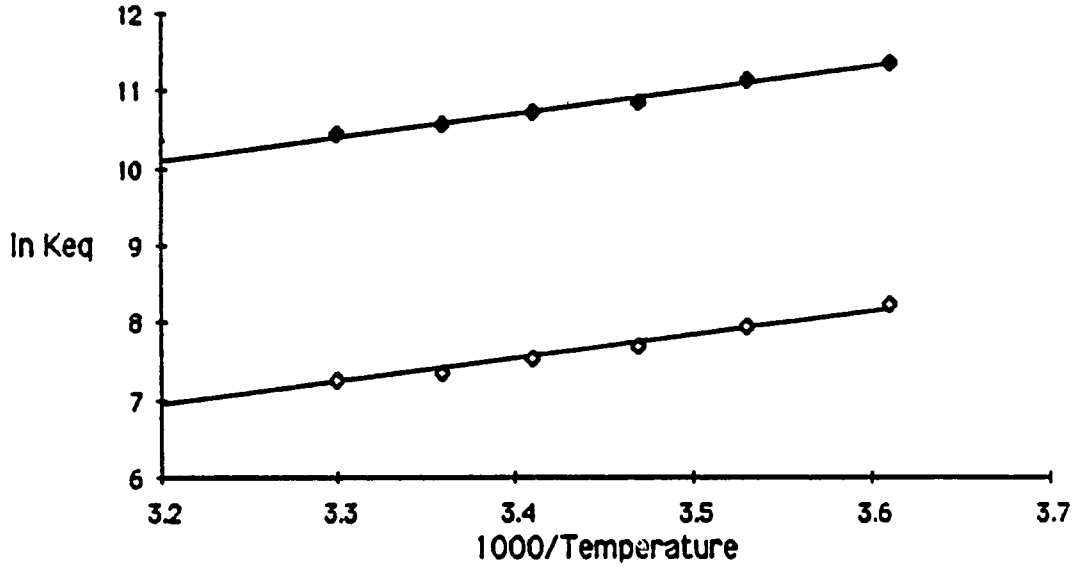
12
11
10
9
8
7
6
ln Keq
3.2
3.3
3.4
3.5
3.6
3.7
1000/Temperature

(b)

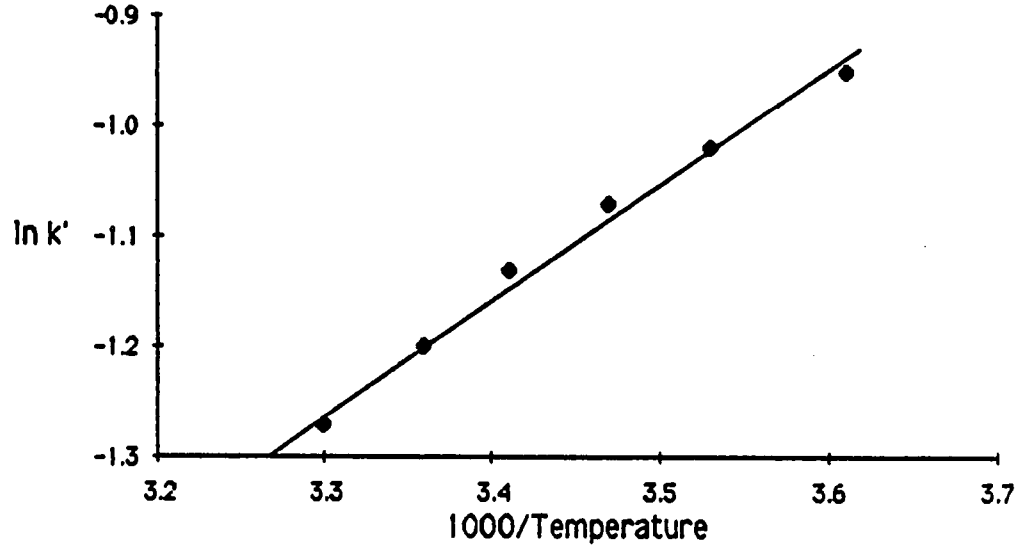
-0.9
-1.0
-1.1
-1.2
-1.3
ln k'
3.2
3.3
3.4
3.5
3.6
3.7
1000/Temperature

by calculating K_3 at each inhibitor concentration from the capacity factor and K_2 at the appropriate temperature using Equation 5 and plotting these K_3 values according to Equation 7 (Figure 3). These values are listed in Table 3. Variation in the values obtained by the two methods could be due to uncertainty in the value of K_2 determined from Figure 1 and used in Equation 5. The $\Delta H°$ values for the Con A - MUM complex are in good agreement with literature values, but there is some difference in $\Delta S°$ values. These facts would be consistent with the assertion that the Con A - MUM interaction is the same in either the homogeneous or heterogeneous system. The same bonds must be broken for the sugar to dissociate, leading to the same $\Delta H°$ value. Immobilization of the Con A results in a loss of conformational freedom, which is reflected in a more positive $\Delta S°$ value.

The excellent agreement for the $\Delta H°$ values determined in the presence of varying concentrations of mannose indicates the presence of the inhibitor does not affect the binding of the complex in a direct manner. The mannose does not displace the bound MUM from the Con A, but only reduces the number of ligand sites that would be available to bind to the MUM. It would be expected that if the inhibitor acted by disrupting the binding, as a chaotropic agent does, differing values of $\Delta H°$ would be obtained.

A comparison between bio-specific interactions and hydrophobic interactions is also shown in Table 3. The $\Delta H°$ of MUGA, which does not bind bio-specifically to Con A, was found to be much smaller than that of any bio-specific interaction. While the hydrophobic interactions between the

Figure 3. Plots used to determine binding enthalpies and entropies at varying inhibitor concentrations. Figure a displays data for 5.02×10^{-5} M mannose, Figure b for 1.00×10^{-4} M mannose, Figure c for 5.24×10^{-4} M mannose and Figure d for 1.00×10^{-3} M mannose.

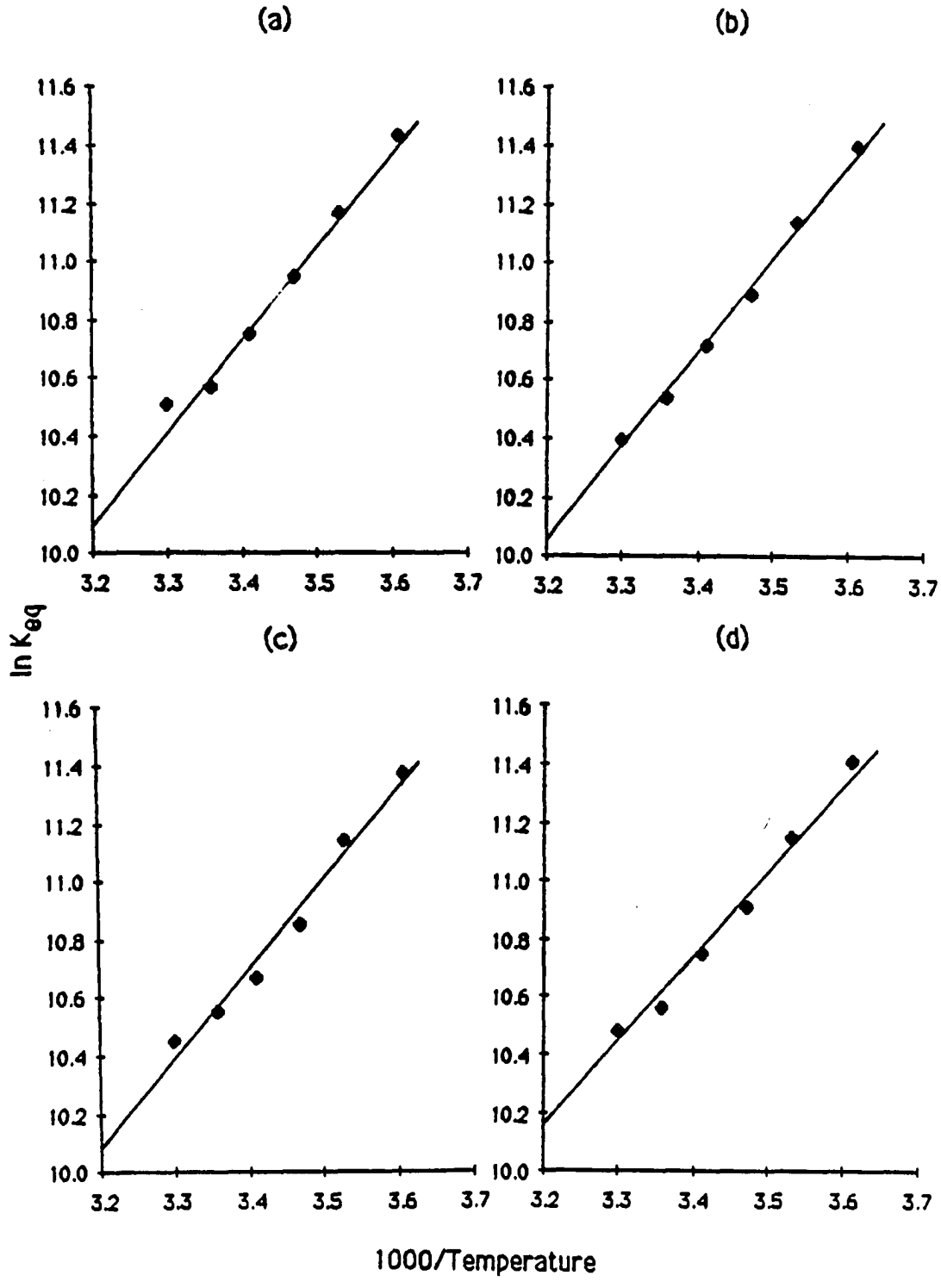
(a)
(b)
(c)
(d)
ln K_{eq}
11.6
11.4
11.2
11.0
10.8
10.6
10.4
10.2
10.0
3.2
3.3
3.4
3.5
3.6
3.7
1000/Temperature

Table 3. Binding Enthalpies and Entropies

System	ΔH° kcal/mol	ΔS° eu
con A-mannose	-6.61 ± 0.44	-7.54 ± 1.52
con A-MUM -[a]	-7.02 ± 0.24	-2.36 ± 1.24
-[b]	-6.15 ± 0.35	0.40 ± 1.20
	-6.16 ± 0.46	0.31 ± 1.59
	-6.62 ± 0.22	-1.29 ± 0.76
	-6.15 ± 0.40	0.44 ± 1.38
-[c]	-8.3 ± 0.1	-7.2 ± 0.3
-[d]	-(6-7)	
con A-MUGA	-2.04 ± 0.09	-9.24 ± 0.31

[a]This work, calculated from Figure 1.
[b]This work, calculated from Equation 5.
[c]Reference 29.
[d]Reference 30.

coumarin rings of MUGA and MUM and the non-polar residues of the Con A are much weaker than the bio-specific interactions, they do provide a measurable retention on the column (k' = 0.30 at 25° C) that must be taken into account in order to obtain accurate equilibrium constant measurements.

Determination of Association Rate Constants by Split-Peak Method

Computer simulations

As discussed in the Introduction, the number of ligand sites are often reduced to increase the probability of split-peak behavior. This also reduces the capacity factor, which causes the adsorption to be reversible in the time scale of the experiment, violating one of the assumptions used in the derivation of Equation 26. A computer simulation was performed to determine what the elution profile of such a system would look like and if any quantitative measurements could be obtained.

Figure 4 shows six elution profiles for a compound with a capacity factor of 5.0 and diffusion/dissociation ratio of 100. The Gaussian shaped peak was generated using 200 slices and corresponds to a column containing 28.8 theoretical plates. As the number of slices was reduced, which corresponds to increasing the flow-rate, the peak became shorter and broader. When some of the analyte began eluting at the void volume, a sharp spike was observed, followed by a large tail. This marks the beginning of the split-peak behavior. The tallest profile corresponds to the situation where half the applied solute elutes in the void volume.

From observations made of Figure 4, it was believed that data could be obtained for situations where the free fraction would exceed 0.3 To obtain data that can be best plotted using Equation 26, the free fraction should fall

Figure 4. Split-peak profiles generated by computer model. Parameters are k_{-1} = 100 iteration^{-1}, k_{-3} = 0.1 iteration^{-1}, k' = 5.0, $V_e = V_p$. Number of slices range from 200 (Gaussian peak) to 5 (tallest peak)

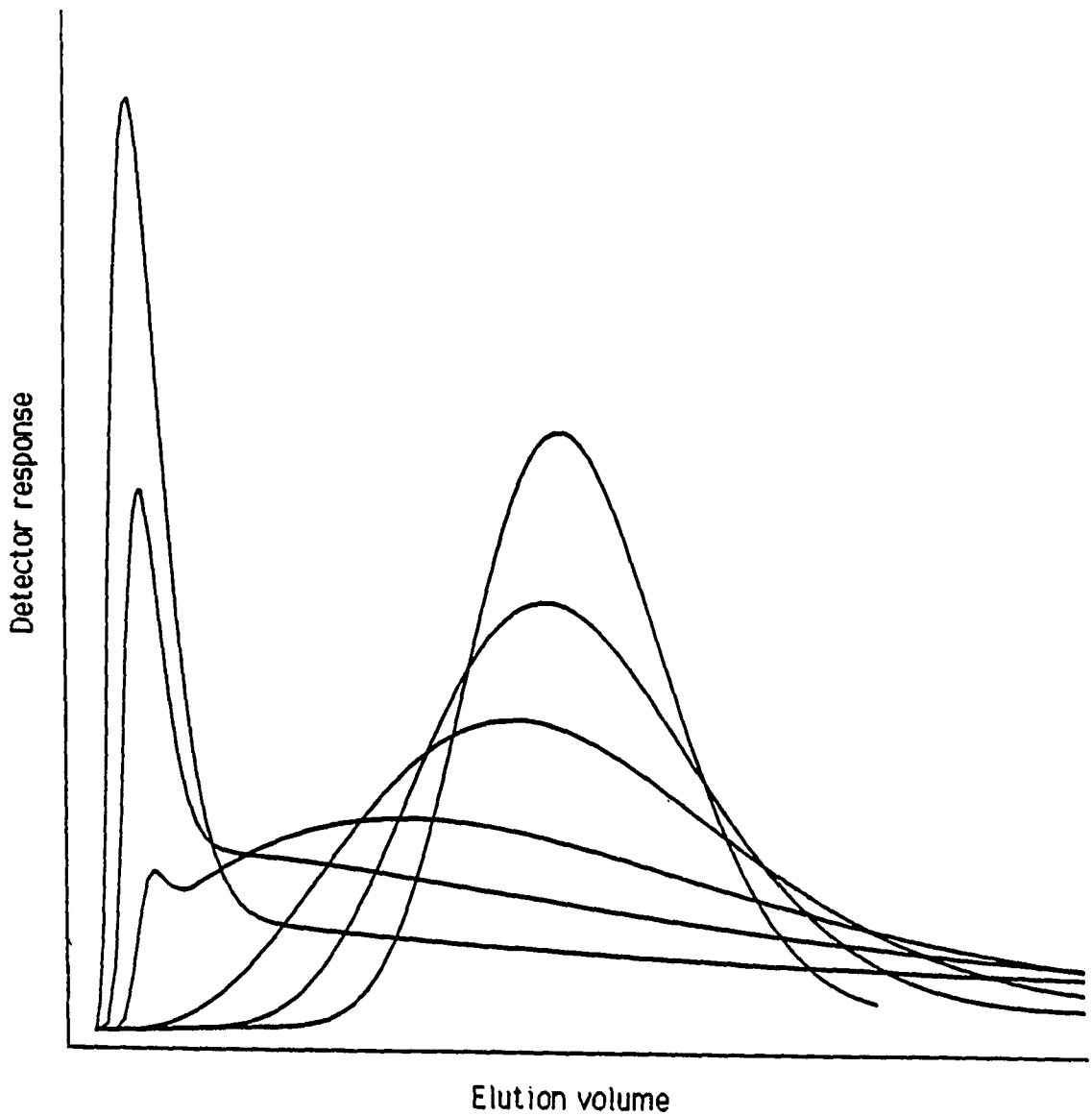
Detector response
Elution volume

in the range of 0.3 to 0.8. This range reduces the effect of any impurity that is either non-retained or strongly retained by the packing material. After deconvolution of the profile into two peaks, the amount of solute that did not interact and the amount that did bind could be obtained. The association rate constant could then be obtained by plotting the free fraction vs. flow-rate according to Equation 26. An anticipated difficulty is distinguishing when all the compound has been eluted from the column. Errors in determining the area of the bound peak can be circumvented by determining the area of the free peak and subtracting from the area of the totally retained peak.

Experimental data

A system consisting of the immobilized protein, Con A, and the sugar PNPM as solute were utilized for the experimental studies. From previous isocratic measurements, approximate rate constants were known: $k_1 \approx 120$ s^{-1}; $k_3 \approx 8.0 \times 10^4$ $M^{-1}s^{-1}$ (11). Calculations using Equation 26 predict that for flow-rates of 1.0 mL/min, 2.2×10^{-10} mole of ligand sites are required to show significant split-peak behavior. Using Equation 5, the calculated void volume to maintain a capacity factor of 5.0 would be 1 µL. Assuming that the total column volume is divided equally between the void volume and the volume of the packing material, the total volume of the column would be 2 µL. A column with dimensions of 4.7 mm x 0.79 mm ID would have a total empty volume of 2.3 µL. From breakthrough curves and protein assay data, the amount of Con A binding sites was estimated to be 1.8×10^{-10} mole.

Figure 5 shows six elution profiles obtained from injections of 3 µL of 6×10^{-6} M PNPM at flow-rates from 0.02 to 1.0 mL/min. As predicted from the computer simulations, the peak became shorter and broader as the flow-rate was increased. At a flow-rate of 1.0 mL/min, the beginnings of split-peak behavior can be seen. However, no data that could be used to determine the association rate constant were obtained due to the disturbance in the baseline from injecting the sample.

In an attempt to obtain useful data, the sugar MUM and fluorescence detection was used in place of PNPM. Fluorescence detectors are not sensitive to the pressure fluctuations caused by the disruption in the flow when the sample is injected. The use of MUM as the solute has the additional advantage of a larger association constant, which enhances the split-peak effect. When the use of a commercial fluorescence detector with a 12-µL flow cell was found to cause significant broadening of the signal, a capillary flow cell was constructed. Use of this flow cell did improve the peak shape, however it was found that reproducible responses could not be obtained. The decision was made to postpone this project until a better detector could be obtained. While this work has not yielded the association rate constant of the immobilized Con A - MUM complex, it has demonstrated that the computer model describes this process at least qualitatively and that the split-peak method may be able to provide kinetic information when adequate detection can be provided.

Figure 5. Experimental split-peak profiles for PNPM eluted from an immobilized Con A column. Flow-rates range from 0.02 mL/min (tallest peak) to 1.0 mL/min

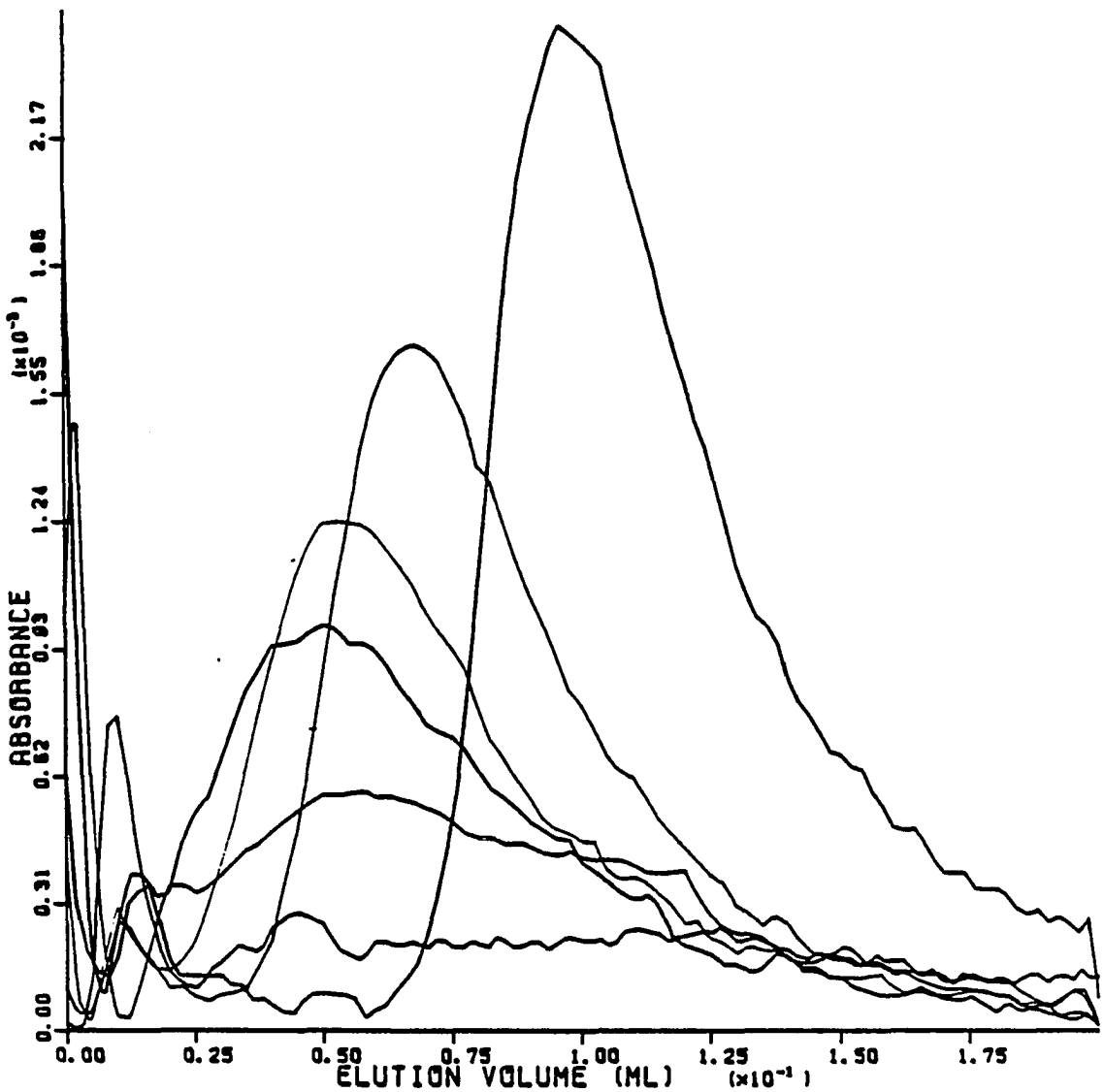
ABSORBANCE
(×10⁻³)
0.00
0.31
0.62
0.93
1.24
1.55
1.86
2.17
0.00
0.25
0.50
0.75
1.00
1.25
1.50
1.75
ELUTION VOLUME (ML)
(×10⁻¹)

Determination of Dissociation Rate Parameters by Peak-Decay Method

Computer simulations

Figure 6 shows two peak-decay profiles, calculated from Equation 32 by using different values of k_{-1}/k_{-3}. Note that when k_{-1} and k_{-3} were similar in magnitude, the peak was broader and the logarithm of the profile was somewhat curved, as expected from the theoretical equation. In such a situation, an aribitrary choice of the portion of the profile to use in determining the slope had to be made. All of the slopes from computer simulations were determined in the following way: the times corresponding to the top of the peak and the point when 99% of the solute was eluted were determined. The time between these points was divided into five equal segments. The slope of the second segment (from the peak) was determined by linear least squares fitting of the points. The segment used is marked in Figure 6. This particular segment was chosen because it most closely duplicated the region used in the experimental data.

Plots identical to Figure 6 were obtained from the two-step reversible computer model when the column length and the capacity factor were both very small. This observation plus the previous split-peak experiments and isocratic experiments (11) support the accuracy of the computer model with respect to the mathematical model of Hethcote and Delisi (17).

The computer model was first used to examine the case in which retention was large enough that significant readsorption could occur but the

Figure 6. Peak-decay profiles (a) and the natural logarithm of the profiles (b) calculated from Equation 32 for the conditions $k_{-1}/k_{-3} = 10$ (taller peak) and $k_{-1}/k_{-3} = 2$ (shorter peak). The vertical marks indicate the region used for slope measurements

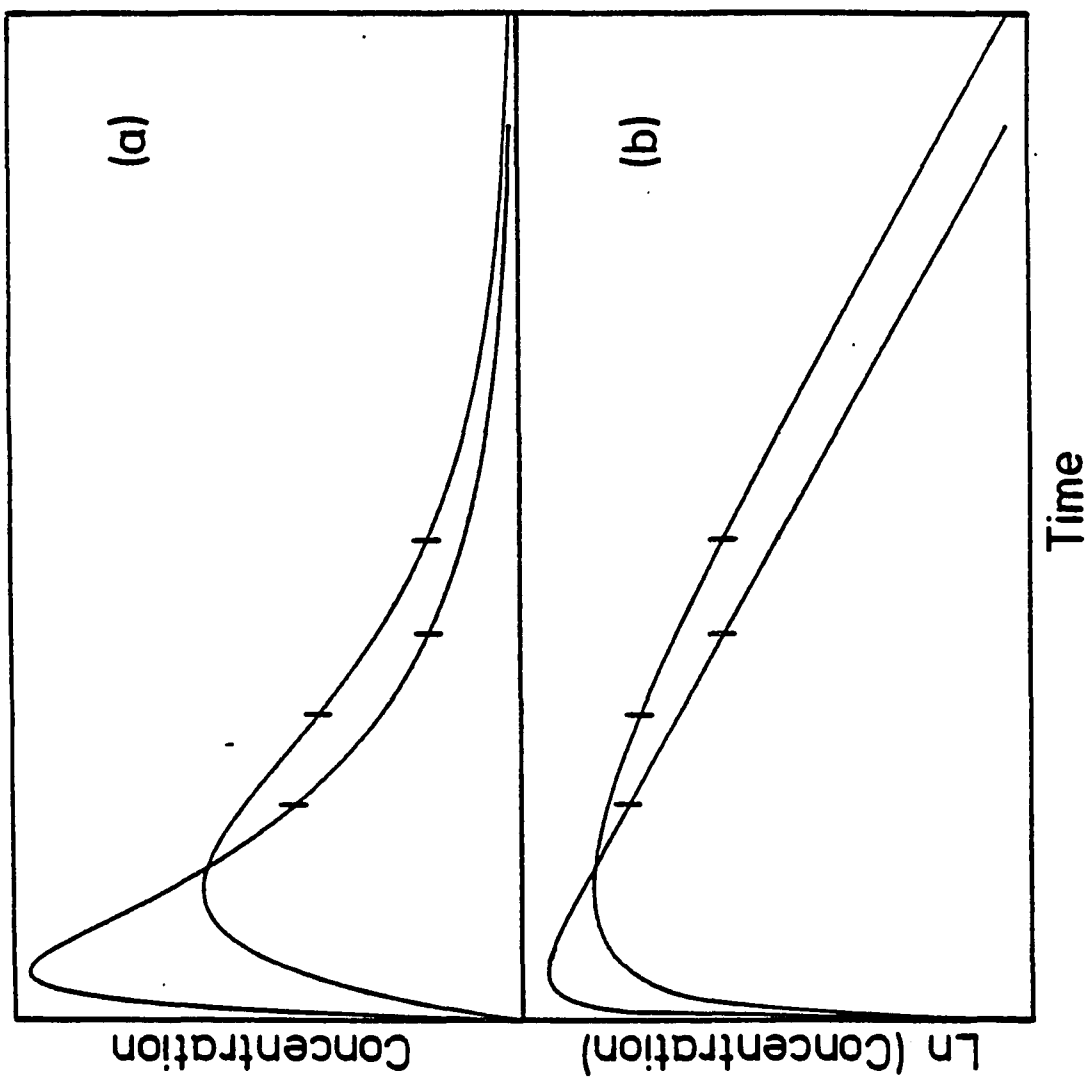
(a)
(b)
Concentration
Ln (Concentration)
Time

column length was still insignificantly small. Rate constants were measured from simulated peak-decay profiles as a function of k' and k_{-1}/k_{-3} (Figure 7). The slopes of the logarithm plots were normalized by dividing by the smaller of the two rate constants. Thus, a normalized slope of 1.00 indicated that the rate constant of the slowest step could be accurately measured. Note that the slopes were always low when k_{-1} was similar in magnitude to k_{-3}. However, if k_{-1} was at least 10-fold larger or smaller than k_{-3}, the the smaller of the two rate constants could be measured with good accuracy when the capacity factor was small.

Figure 7 also shows that the accuracy of the apparent rate constants declined as the capacity factor increased. This is because multiple adsorption and desorption steps began to take place and caused additional band-broadening. Interestingly, at high capacity factor values, the plot was very asymmetric and indicated that when $k_{-1}/k_{-3} > 100$, k_{-3} could still be accurately determined, but when $k_{-1}/k_{-3} < 0.01$, k_{-1} could not be determined accurately. This difference was due to the fact that in the former case, as soon as the adsorbed complex dissociated, the solute immediately diffused out of the pore and was washed from the column. In the latter case, adsorbed solute and free solute in the pore volume were essentially in equilibrium, and so the solute diffused out of the pore more slowly than if all the solute were free.

Figure 7. Plot of normalized slope from computer simulations of peak-decay profiles as a function of k_{-1}/k_{-3} and k' for $V_p/V_e = 0.1$ and zero column length

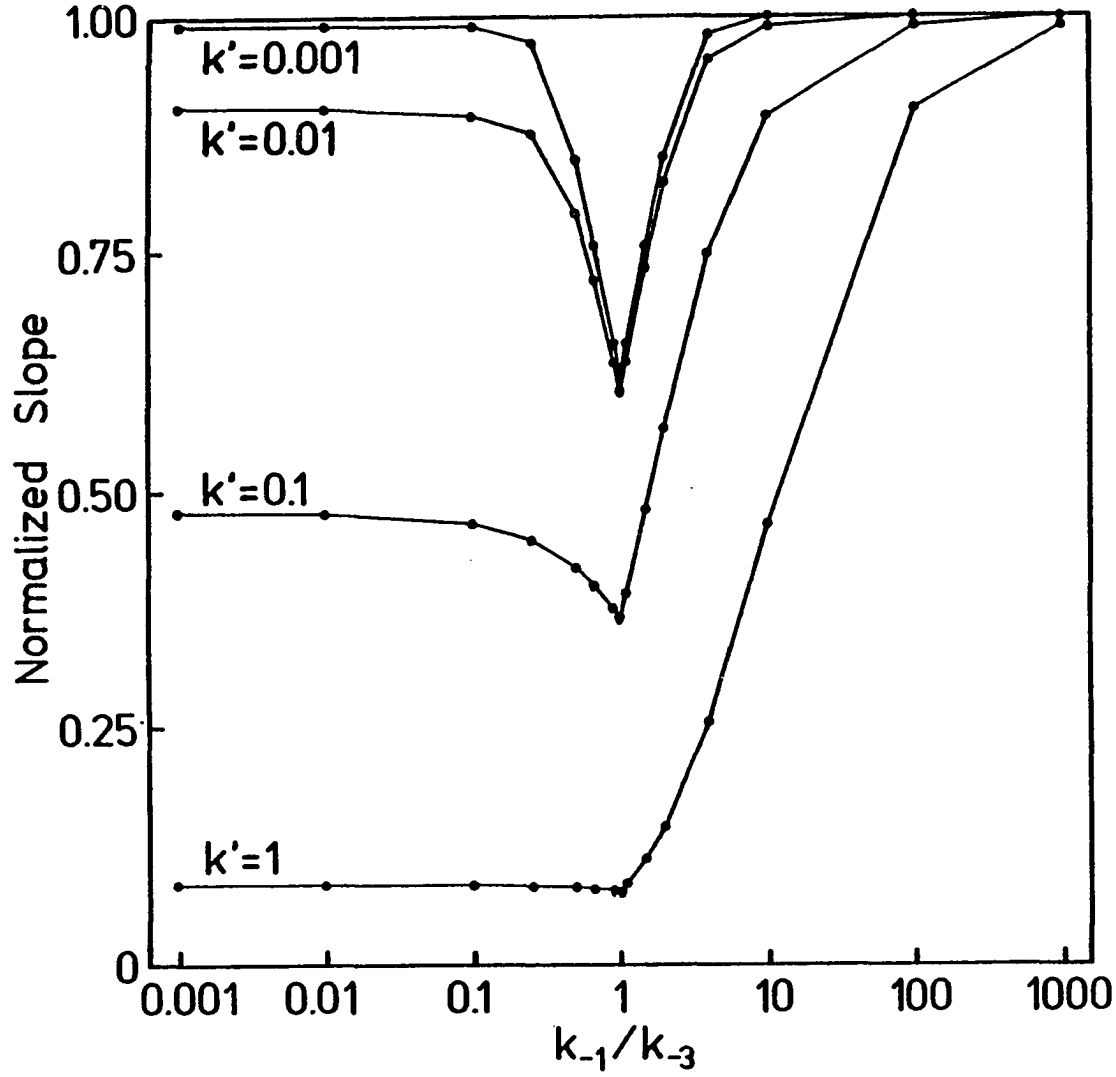
1.00
0.75
0.50
0.25
0
Normalized Slope
k'=0.001
k'=0.01
k'=0.1
k'=1
0.001
0.01
0.1
1
10
100
1000
k-1/k-3

Plots drawn with different values of V_p/V_e were similar to Figure 7 but shifted vertically. Examination of the data indicated that plotting the data as a function of $k'V_m/V_p$ caused the data generated at different V_p/V_e values to merge into a single family of curves. From such a plot it was possible to determine the maximum allowable value of $k'V_m/V_p$ such that the adsorption or desorption rate constant could be determined accurately.

As the column length increased to significant values (Figure 8), there was a greater likelihood of multiple adsorption-desorption steps with the result that the elution profiles became less steep. This was, in fact, not a function of the column length, but rather of the residence time of the solute in the column (i.e., the void time, t_m) relative to the rate constants. The factor V_m/V_p also was important here; hence, the normalized slope is plotted in Figure 7 vs. the product of t_m, V_p/V_m and the smaller of the two rate constants (k_{-1} or k_{-3}). From this plot, the maximum allowable void time could be determined.

By examination of the data used to prepare Figures 6 and 7, conditions were found such that the smaller of the two rate constants could be measured with less than a 5% error. The conditions for accurate determination of the diffusion rate constant, k_{-1} were:

$$\frac{k_{-1}}{k_{-3}} \leq 0.1 \qquad (31)$$

Figure 8. Plots of normalized slope from computer simulations of peak-decay profiles as a function of void time for k_{-1}/k_{-3} = 0.1 (a), 1.0 (b) and 10.0 (c). From top to bottom, the curves represent 10-fold increases in $k'V_m/V_p$ beginning at a value of 0.02 for V_m/V_p = 2 (solid symbols) and V_m/V_p = 10 (open symbols)

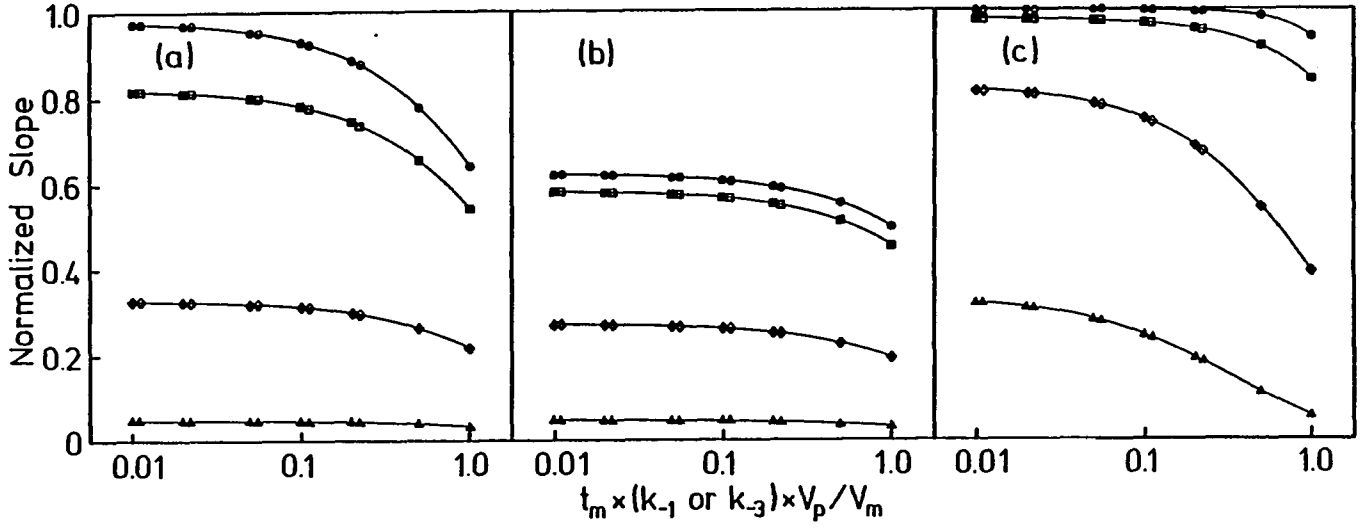
(a)
(b)
(c)
Normalized Slope
1.0
0.8
0.6
0.4
0.2
0
0.01
0.1
1.0
$t_m \times (k_{-1}$ or $k_{-3}) \times V_p / V_m$

$$\frac{t_m k_{-1} V_p}{V_m} \leq 0.05 \tag{32}$$

$$\frac{k' V_m}{V_p} \leq 0.02 \tag{33}$$

The conditions for the accurate measurement of the dissociation rate constant, k_{-3} were:

$$\frac{k_{-1}}{k_{-3}} \geq 10 \tag{34}$$

$$\frac{t_m k_{-3} V_p}{V_m} \leq 0.2 \tag{35}$$

$$\frac{k' V_m}{V_p} \leq 0.2 \tag{36}$$

Other conditions may also be acceptable. For example, if $k_{-1}/k_{-3} \geq 100$, the

Figure 7 shows that the requirement for capacity factor could be relaxed somewhat.

Figure 9 shows two peak profiles generated from the computer model. One was the nearly ideal case in which $k_{-1}/k_{-3} = 1.0$, $V_p/V_e = 1$, $t_m k_{-3} = 0.02$ and $k' = 0.01$. The normalized slope was 0.998, i.e., only 0.2% less than the expected value. The other curve was for a case where $t_m k_{-3} = 2$ and $k' = 1.0$. The normalized slope decreased to 0.386 and thus the apparent rate constant was significantly less than the expected value.

If there were heterogeneity in the values of either of the two rate constants, then Equation 32 could be expanded to include more terms, each with its own number of binding sites and diffusion and dissociation rate constants. The logarithm plots would then be the sum of several exponential terms, leading to a plot which flattens as time increases (just the opposite of Figure 6b, where the plot became steeper with time).

If the slope were measured late in the tail of the peak, it always approached the smallest of the individual rate constants because the faster decaying solute molecules had already left the column. If the slope were measured as described earlier, the apparent rate constant turned out to be quite close to the apparent value that would have been obtained from an isocratic experiment, i.e., weighted toward the smallest rate constant.

Figure 9. Computer-simulated peak-decay profiles (a) and the natural logarithms of the profiles (b) for $k_{-1}/k_{-3} = 10$ and $V_p/V_e = 1$. For the taller peak, $t_m k_{-3} V_p/V_m = 0.01$ and $k' V_m/V_p = 0.02$. For the shorter peak, the quantities are 1.0 and 2.0, respectively

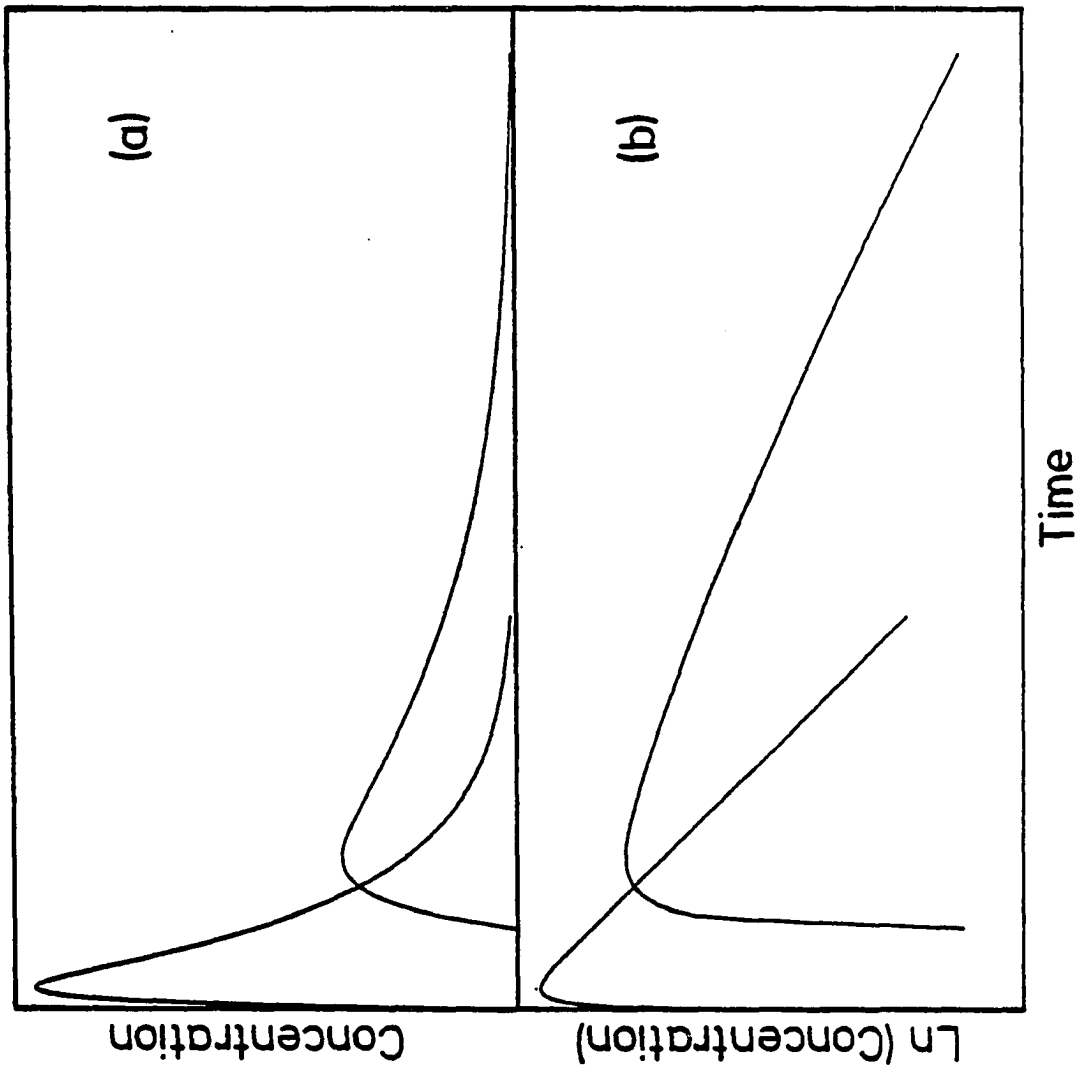
(a)
(b)
Concentration
Ln (Concentration)
Time

Determination of immobilized Con A - MUM complex dissociation rate constant

The system consisting of immobilized protein, Con A, as the ligand and the sugars MUM and mannose as the solute and inhibitor, respectively, was utilized for the experimental studies. From previous isocratic measurements, approximate values of the rate constants were known: $k_{-1} \approx 120\ s^{-1}$; $k_{-3} \approx 2\ s^{-1}$ (11). The ratio of the rate constants easily met the criterion of Equation 34. For the Hypersil column used, the ratio of pore volume to void volume was approximately 0.44. Thus Equation 35 required the void time to be no greater than 0.23 s. This was a severe requirement, and therefore high flow-rates and/or small columns were needed to measure a dissociation rate this fast. A 6.3 mm x 2.1 mm I.D. column was chosen. With a void volume of approximately 14 µL, the needed flow-rate was calculated to be 3.7 mL/min. To meet the criterion of Equation 36 required a capacity factor no greater than 0.088. From the isocratic studies described in this dissertation, the binding constants for the sugars were determined: K_3 (MUM) = 45000 M^{-1}; K_2 (mannose) = 1500 M^{-1}. From breakthrough curve and protein assay data, the number of moles of active Con A in the column was estimated to be 18 nmol. From Equation 3 of reference 11, the minimum inhibitor concentration was calculated to be 0.44 M.

Figure 9 shows the data from a typical experimental run at a flow-rate of 10 mL/min and 0.1 M mannose concentration. The logarithmic plots

Figure 10. An experimental peak-decay profile (a) and natural logarithm of the profile (b) for MUM eluted from an immobilized Con A column at a flow-rate of 10 mL/min with a mannose concentration of 0.1 M. The vertical marks indicate the region used for slope measurements.

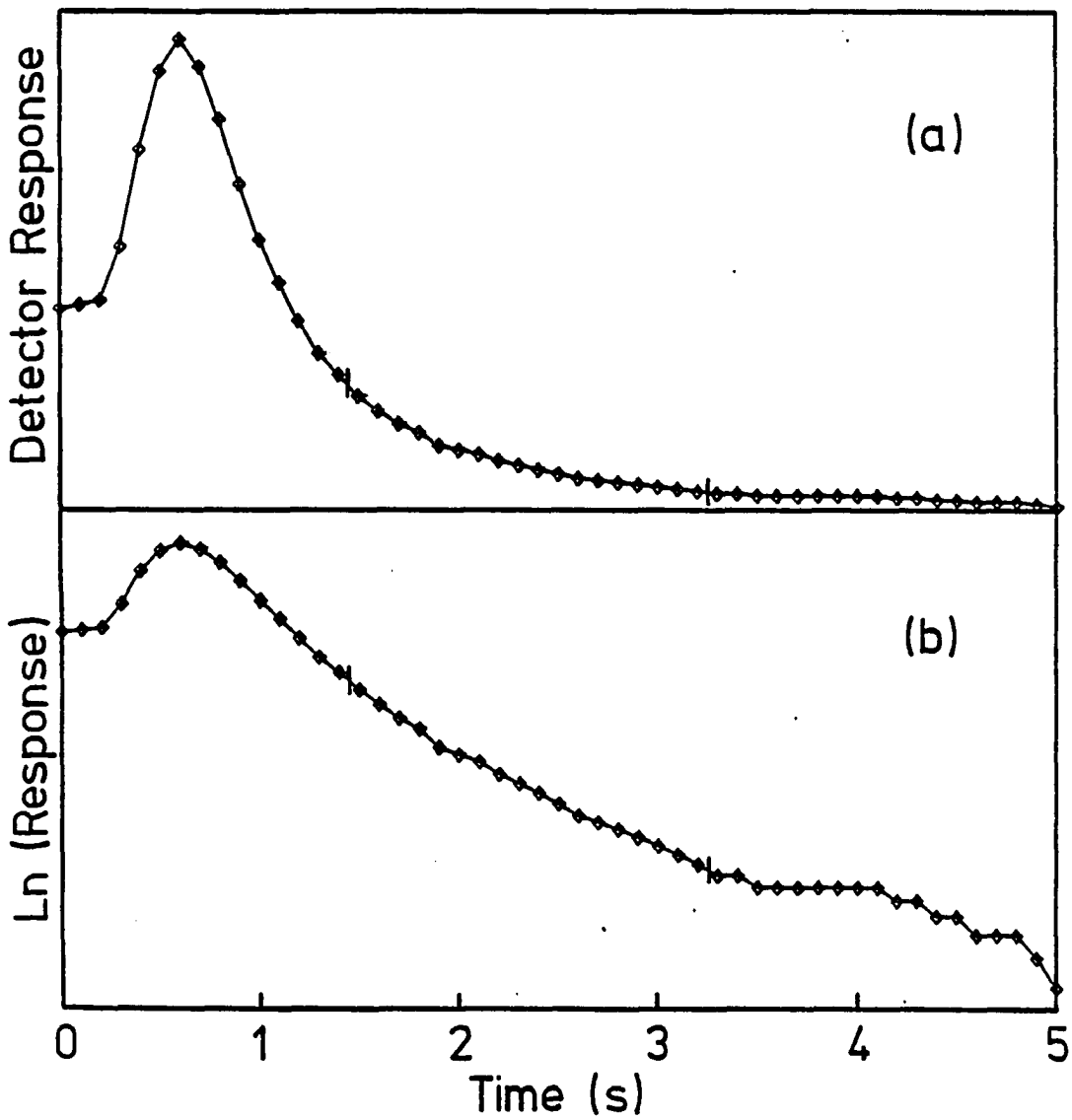
Detector Response
(a)
Ln (Response)
(b)
0
1
2
3
4
5
Time (s)

(Figure 10b) typically were somewhat concave, but the slope could be determined with excellent precision [± 3% relative standard deviation (R.S.D.) from the slope of a single run, ± 5% R.S.D. for replicate runs]. As pointed out earlier, one possible cause of the concave plot could be heterogeneity in the immobilized Con A.

Experiments were performed at several flow-rates (Figure 11) and mannose concentrations (Figure 12) to determine whether the data obeyed Equations 35 and 36. Both experiments exhibited the expected trends, with the apparent rate constants reaching a plateau value of approximately 1.78 s^{-1} at high flow-rate (small t_m) and high inhibitor concentration (small k').

The flow-rate and inhibitor concentration needed to reach the plateau value of the dissociation rate constant were somewhat different than those predicted above. To examine this further, the experimental system was modeled with the parameters listed above and a value of 1.82 s^{-1} for k_{-3}. The simulated data are also shown in Figures 11 and 12. From Figure 11, it is apparent that the model predicted only a small change in the apparent rate constants over the flow-rate range used, whereas the actual change was much greater. The difference was probably caused by factors not taken into account in the model, such as dispersion of the inhibitor front as it passed through the column, or eddy diffusion/mobile-phase mass-transfer effects on the solute band-broadening. On the other hand, Figure 12 shows better agreement between experimental and predicted values of the dissociation rate constant as a function of inhibitor concentration. Some of the discrepancies between theory and experiment in both Figures 11 and 12 could be due to

Figure 11. Experimental (●) and theoretical (■) plots of the apparent dissociation rate constant vs. flow-rate for the Con A - MUM system with 0.1 M mannose as inhibitor.

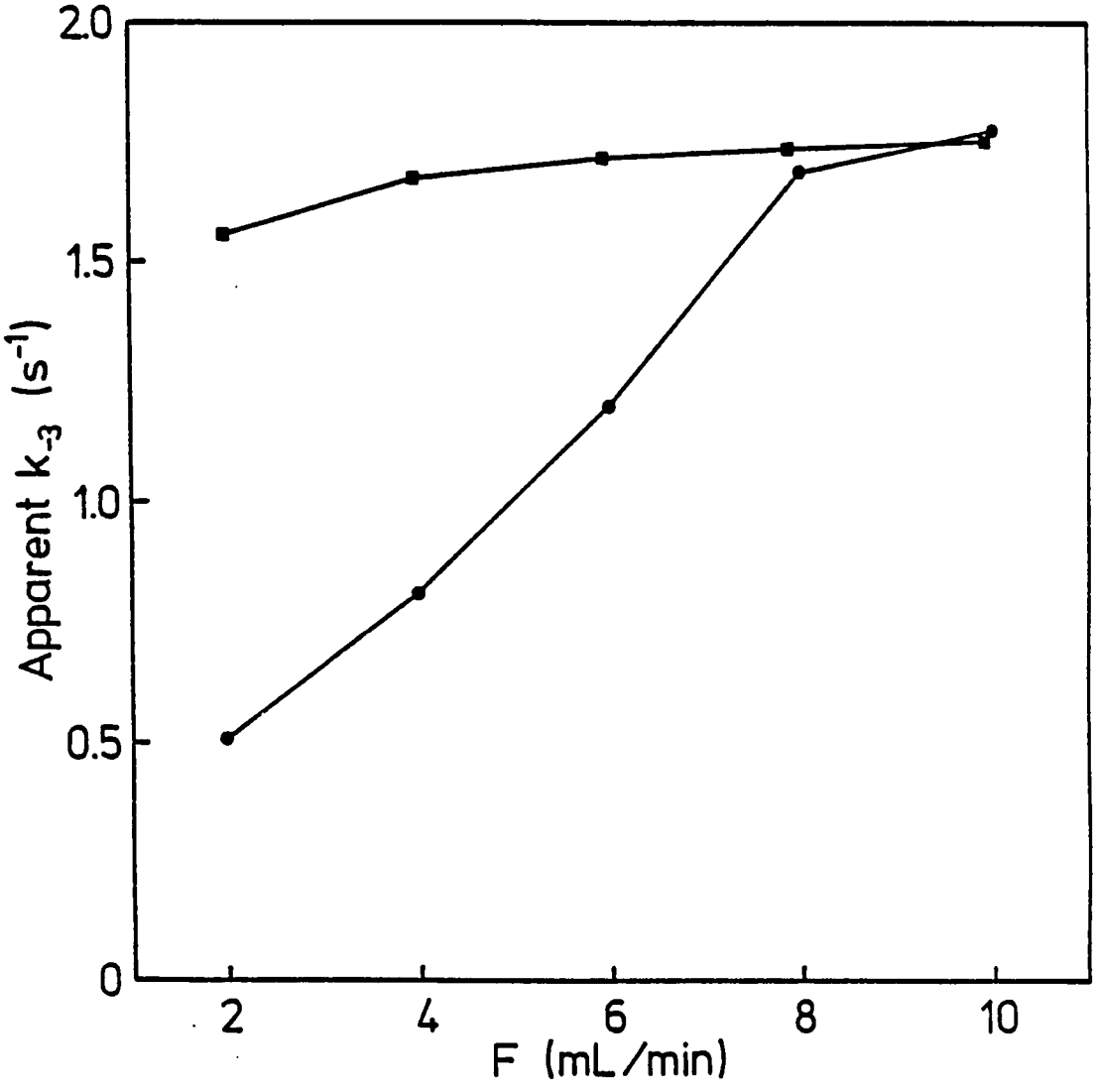
2.0
1.5
1.0
0.5
0
Apparent k_{-3} (s^{-1})
2
4
6
8
10
F (mL/min)

Figure 12. Experimental (●) and theoretical (■) plots of the apparent dissociation rate constant vs. inhibitor concentration for the Con A - MUM system at a flow-rate of 10 mL/min.

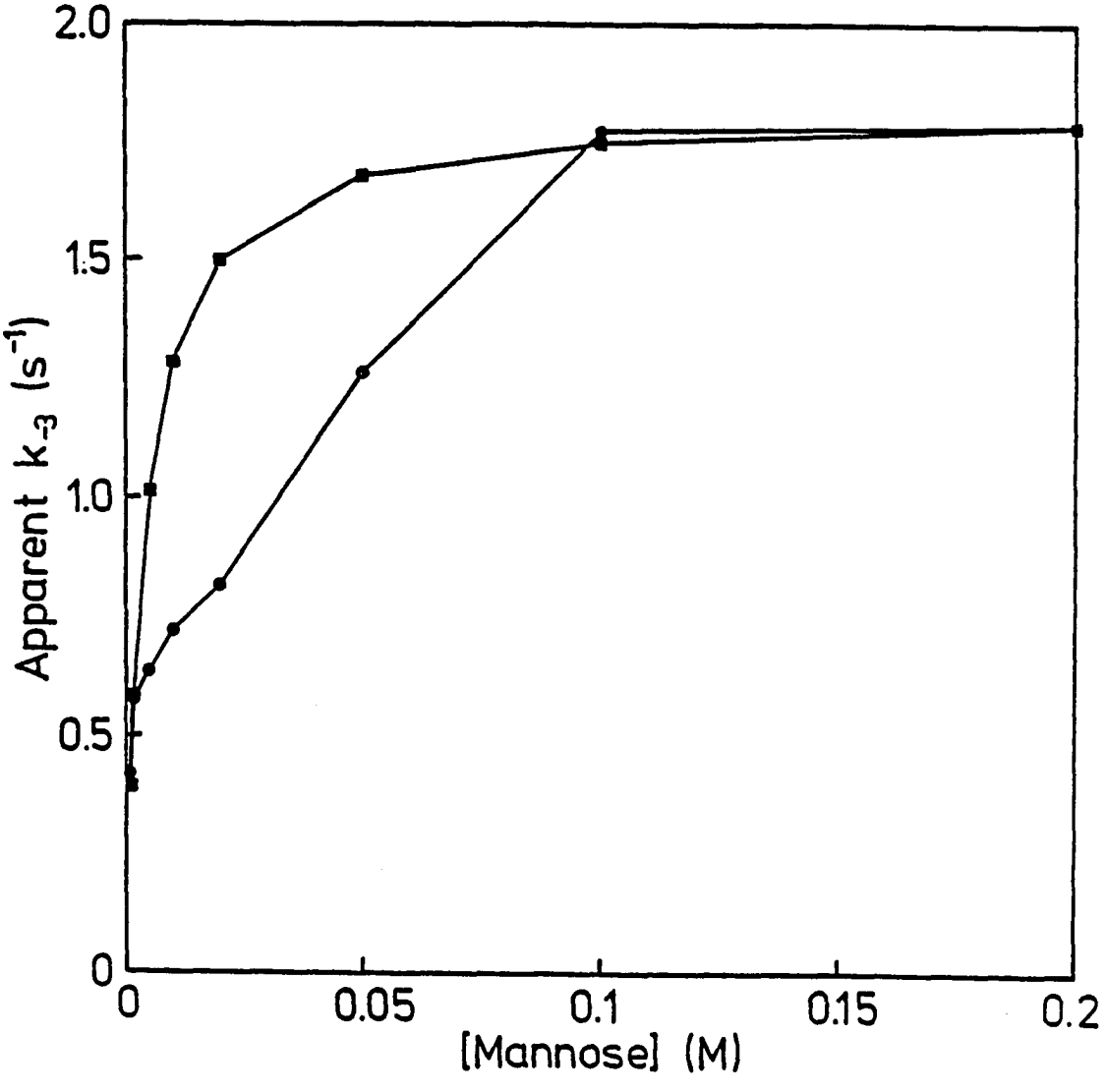
2.0
1.5
1.0
0.5
0
Apparent k_{-3} (s^{-1})
0
0.05
0.1
0.15
0.2
[Mannose] (M)

inaccuracies in the values of void volume, number of active sites, etc., used in the simulations.

Another factor examined was the effect of washing the column with buffer to remove excess MUM prior to the step change in mobile phase. The calculated capacity factor for the MUM in the absence of inhibitor was 58. It is apparent that with the small void volume of the column, all the MUM would be eluted isocratically in a relatively short time period. To examine this, the length of the wash time was varied from 2 to 5 min at 1.0 mL/min. The rate constants were measured using a flow-rate of 10.0 mL/min and 0.1 M mannose. Table 4 shows the results of this study. No change in the rate constant was observed for wash times of between 2.5 and 4 min. The apparent change at longer wash times may have been due to experimental error in the data, as the amount of MUM remaining in the column declined.

Taking into account column-to-column reproducibility, the dissociation rate for the immobilized Con A - MUM complex was $1.8 \pm 0.1\ s^{-1}$ at 25° C. This is in excellent agreement with a value of $2.0 \pm 0.6\ s^{-1}$ as determined by isocratic studies (11) and in fair agreement with a value of $3.4\ s^{-1}$ from free solution studies (30). Since the equilibrium binding constant appears to be larger for immobilized Con A, the values of the association rate constant calculated from Equation 9 for immobilized Con A ($8.1 \times 10^4\ M^{-1}s^{-1}$) and free Con A ($11.2 \times 10^4\ M^{-1}s^{-1}$) are in good agreement.

Table 4. Effect of Column Washing prior to Elution of MUM

Wash time (min)	Apparent k_{-3} (s^{-1})	Relative peak area
2.0	1.54	1.00
2.5	1.79	0.40
3.0	1.77	0.31
3.5	1.75	0.21
4.0	1.76	0.13
4.5	1.10	0.09
5.0	1.18	0.06

Determination of activation parameters of immobilized Con A - MUM complex

Dissociation rate constants for the temperature range of 4° to 30° C for the immobilized Con A - MUM complex utilizing the peak-decay method. Association rate constants were then calculated from these values and the equilibrium constants determined from isocratic zonal elution. The values are listed in Table 5. Although the dissociation rates were observed to increase as the temperature increases, no apparent trend is observed in the association rate. This apparent lack of temperature dependency would indicate that any change in the association rate is smaller than the precision of the measurements obtained.

The activation energy and the enthalpy of activation were calculated from plots of the Arrhenius and Eyring equations (31), respectively (Figures 12 and 13). The values are shown in Table 6. A comparison with the literature solution data shows that the rate constant for the immobilized Con A - MUM complex is approximately a factor of two smaller than the solution values, and the E_a and ΔH^* are also a factor of two smaller than the corresponding solution values. Three explanations could be suggested to solve this seeming contradiction. If the measurements used to calculate the rate constant of the Con A - MUM complex in solution or when immobilized are not sufficiently precise, any estimate of E_a or ΔH^* would be subject to considerable error. However, the indicated precision of Clegg et al. (30) and of this work are sufficient to provide accurate measurements. An alternate explanation is that readsorption takes place after the MUM dissociates from the immobilized

Table 5. Equilibrium and Rate Constants for the Con A - MUM Complex

Temperature °C	K_{eq} (M^{-1})	$k_{dissoc.}$ (s^{-1})	$k_{assoc.}$ ($M^{-1}s^{-1}$)
4	104,000	0.6 ± 0.1	67,000
10	81,000	0.8 ± 0.1	66,000
15	62,800	0.9 ± 0.1	57,000
20	53,400	1.3 ± 0.1	68,000
25	45,000	1.8 ± 0.1	80,000
	33,000 [a]	3.4 ± 0.1 [a]	110,000 [a]
30	34,100	2.0 ± 0.1	67,000

[a] Reference 30.

Figure 13. Temperature dependence of dissociation rate constant as determined by the Arrhenius equation

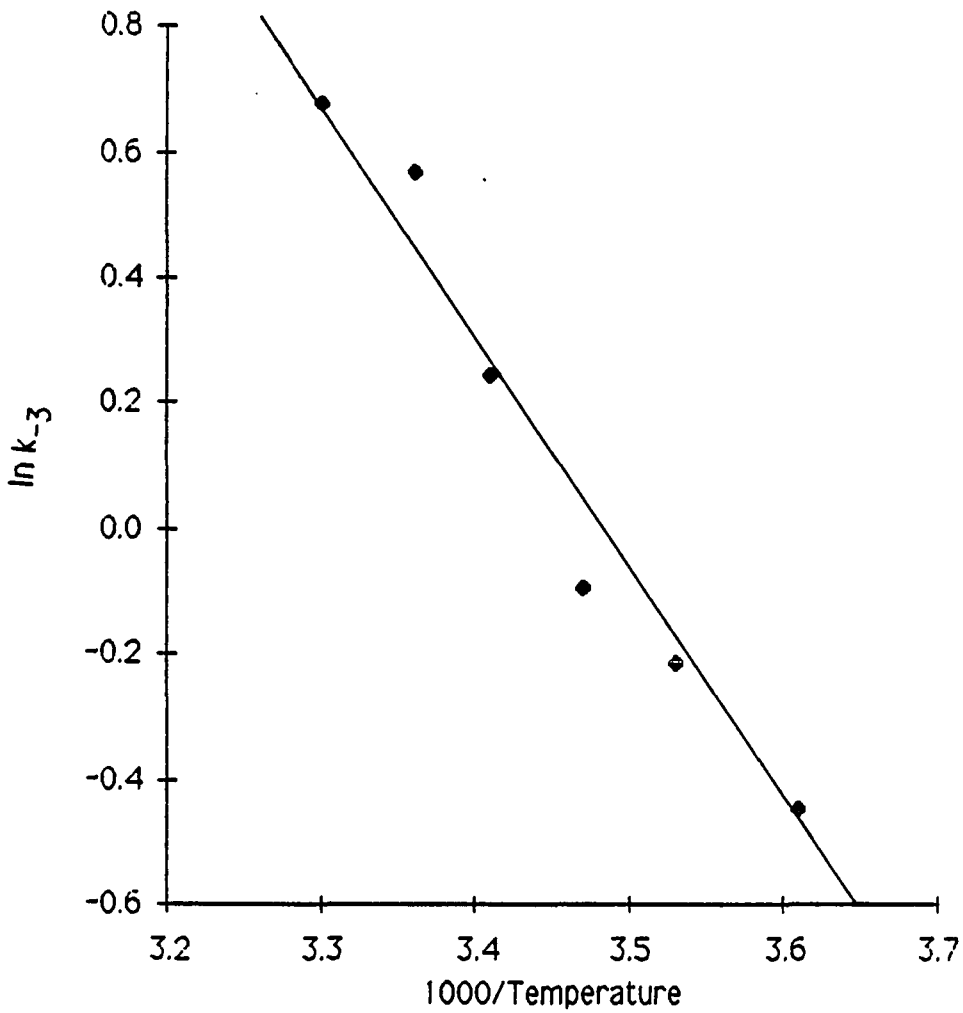
0.8
0.6
0.4
0.2
0.0
-0.2
-0.4
-0.6
ln k-3
3.2
3.3
3.4
3.5
3.6
3.7
1000/Temperature

Figure 14. Temperature dependence of dissociation rate constant as determined by the Eyring equation

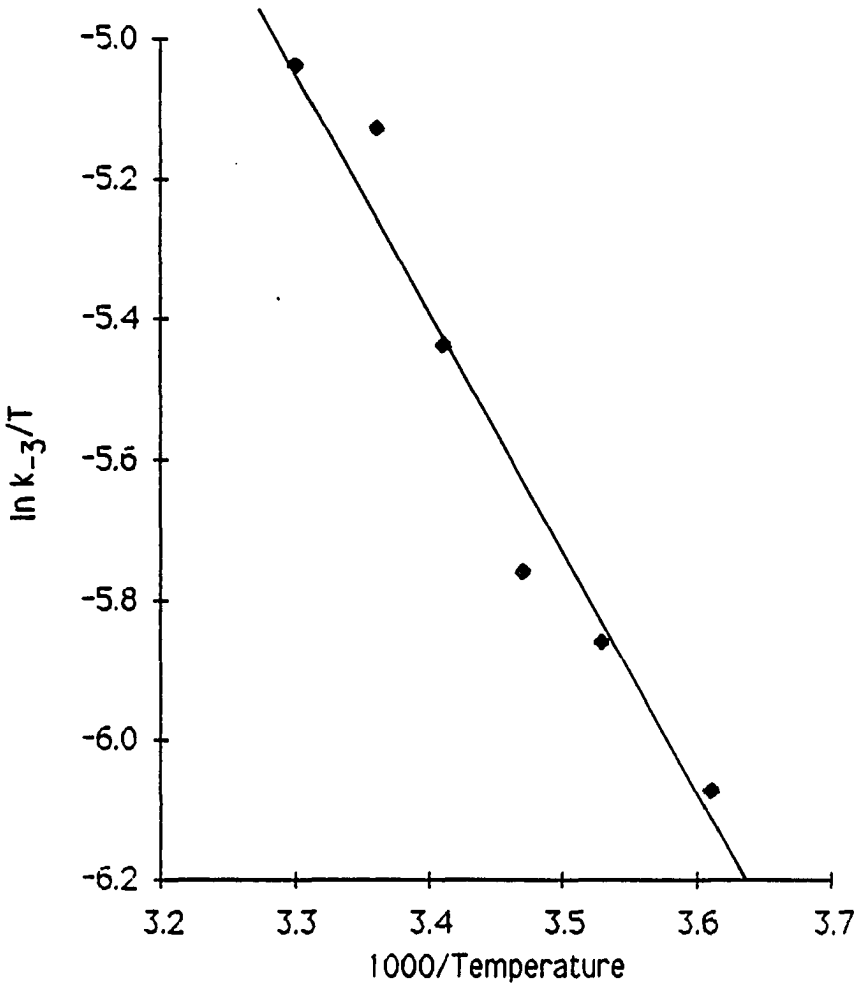
-5.0
-5.2
-5.4
-5.6
-5.8
-6.0
-6.2
ln k-3/T
3.2
3.3
3.4
3.5
3.6
3.7
1000/Temperature

Table 6. Activation Parameters for Dissociation of Con A - MUM Complex

ΔH^* kcal/mol	ΔS^* eu	E_a kcal/mol	Reference
7.2 ± 0.7	-43.4 ± 0.3	7.7 ± 0.7	t.w.
14.3 ± 1.0	-41.3 ± 0.2	14.9 ± 1.0	21

Con A but before the MUM molecule can diffuse from the pore. The elution would then be described by the reactions:

$$E\text{-}L \underset{k_3^*}{\overset{k_{-3}}{\rightleftarrows}} E_p \xrightarrow{k_{-1}} E_m \tag{36}$$

The apparent rate constant for this process can be shown to be (19):

$$\frac{dE_m}{dt} = \frac{k_{-1}k_{-3}E_0}{\lambda_2 - \lambda_3}\left(e^{-\lambda_3 t} - e^{-\lambda_2 t}\right) \tag{37}$$

where

$$\lambda_2 = (p + q)/2 \tag{38}$$

$$\lambda_3 = (p - q)/2 \tag{39}$$

and

$$p = k_3^* + k_{-3} + k_{-1} \tag{40}$$

$$q = \sqrt{p^2 - 4k_{-3}k_{-1}} \tag{41}$$

The readsorption would cause the apparent rate constant to be lower than the actual rate constant and a value determined for the activation enthalpy would be in error. However, readsorption introduces significant error only when the readsorption rate approximates the diffusion rate constant. The calculated value of this pseudo-first order constant is approximately 1% of that of the diffusion rate and would cause less than 0.5% error in the value for the dissociation rate constant.

A third explanation results from a closer investigation of the desorption and diffusion processes, as diagramed in Figure 15. After dissociation, the MUM molecule must diffuse from the stagnant mobile phase into the moving mobile phase. While diffusion is much faster kinetically than the dissociation, any energy required would affect the apparent kinetic parameters:

$$\Delta H^{*}_{apparent} = \Delta H^{*}_{dissociation} + \Delta H^{\circ}_{diffusion}. \qquad (42)$$

If the diffusion from the stagnant mobile phase is an endothermic process, the overall effect would be a lower apparent activation energy for a kinetically slower process. To accurately measure the enthalpy of activation, diffusion would need to be eliminated. The use of a non-porous support would reduce, but not eliminate, the amount of stagnant mobile phase.

Figure 15. Reaction coordinate for dissociation and diffusion of immoblilzed Con A - MUM complex

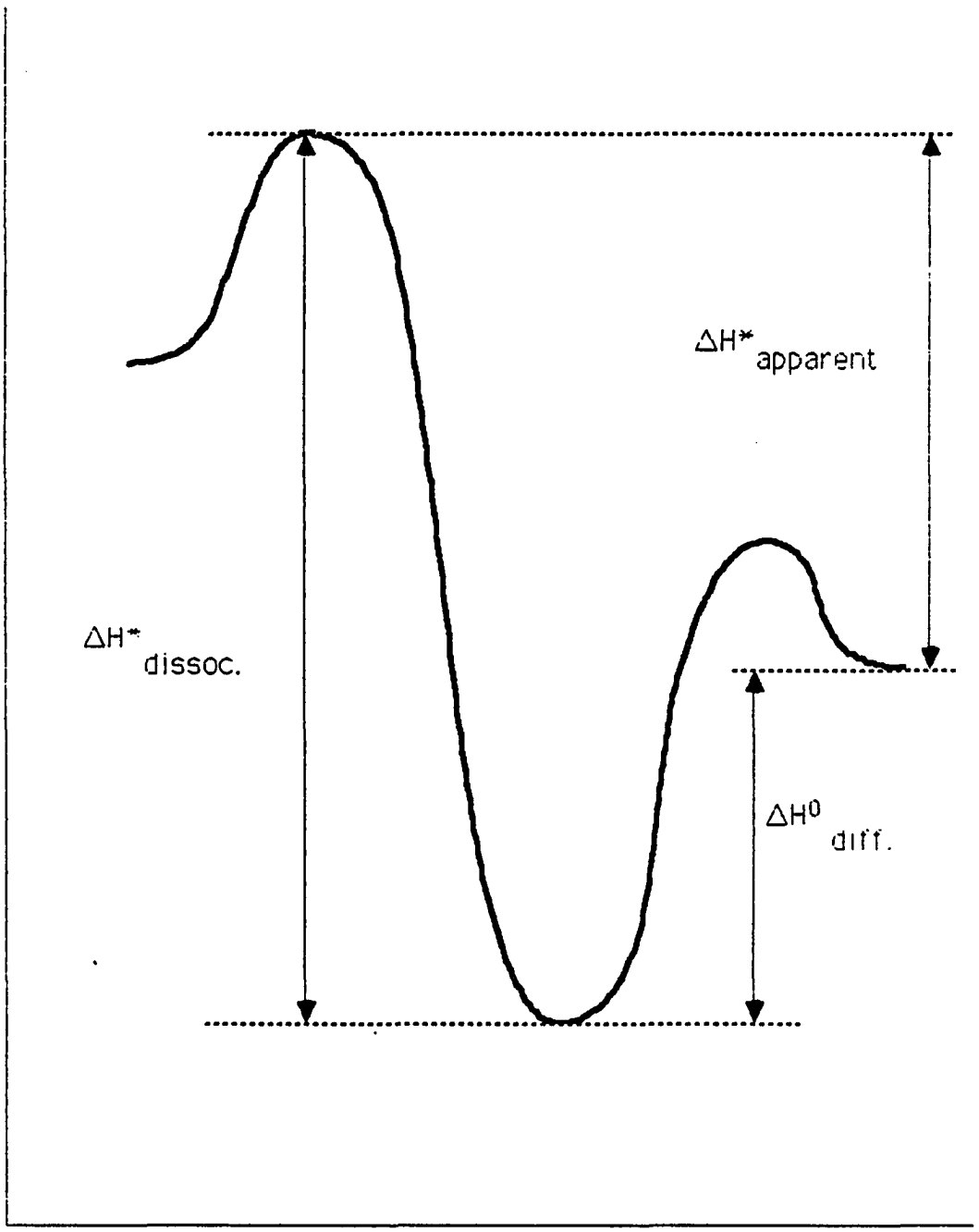
ΔH* apparent
ΔH* dissoc.
ΔH⁰ diff.

Determination of the rate constant for the Con A - PNPM complex

The dissociation rate constant of the immobilized Con A - PNPM complex was determined using the peak-decay method. Flow-rate and inhibitor concentration similar to those reported in Figures 10 and 11 were performed to verify the conditions required for accurate measurements of the dissociation rate (Figures 16 and 17). A flow-rate of 10 mL/min and inhibitor concentration of 0.1 M mannose were found to be required before the observed rate constant reached its limiting value. Taking into account column-to-column reproducibility, the dissociation rate for the immobilized Con A - PNPM complex was 2.6 ± 0.1 s^{-1} at 25° C. This is in good agreement with a value of 3.4 ± 0.4 s^{-1} as determined by isocratic studies (11) but is less than half of a value of 6.2 s^{-1} from solution studies (32).

Effect of immobilization method on desorption kinetcs

Hage et al. demonstrated that the manner in which the protein ligand is attached to the support has a profound effect on the adsorption kinetics of the immobilized protein A - IgG complex (14). The effect of the immobilization method on the desorption kinetics of the Con A - MUM were investigated by measuring the dissociation rate constant when either the Schiff base (25) or the carbonyldiimidazole (26) method were used to immobilized the Con A. The averages of at least 15 determinations on three columns for each method are listed in Table 7. There is no statistical difference in either the mean value or the standard deviation between the

Figure 16. Effect of flow-rate on the apparent dissociation rate constant of the Con A/PNPM system with 0.1 M mannose as inhibitor

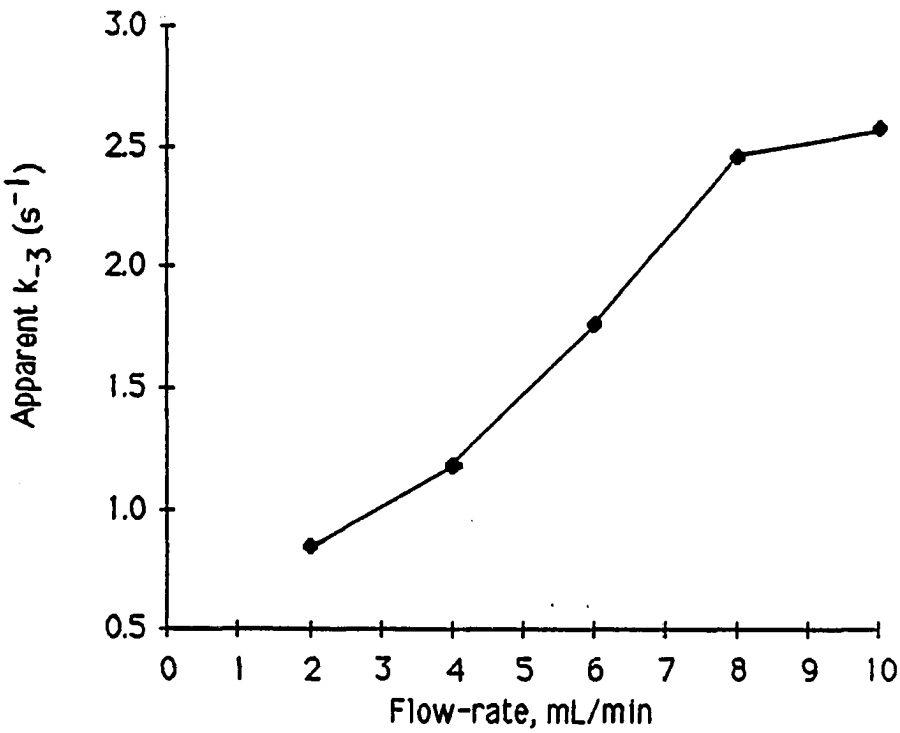
3.0
2.5
2.0
1.5
1.0
0.5
Apparent k_{-3} (s^{-1})
0
1
2
3
4
5
6
7
8
9
10
Flow-rate, mL/min

Figure 17. Effect of inhibitor concentration of the apparent dissociation rate constant of the Con A/PNPM system with a flow-rate of 10 mL/min

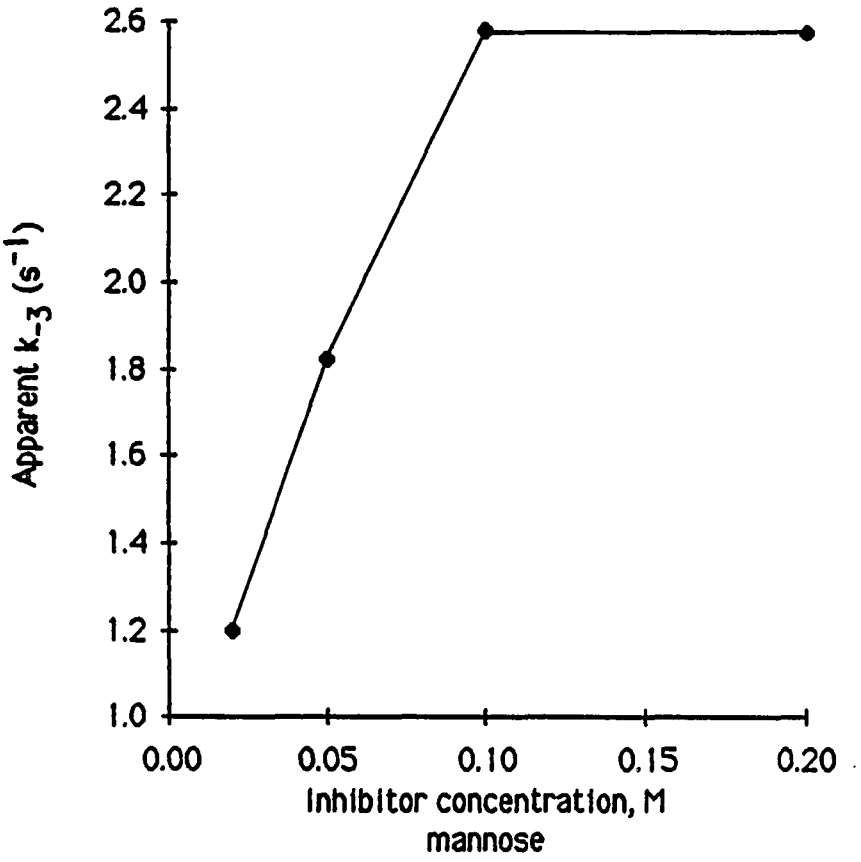
2.6
2.4
2.2
2.0
1.8
1.6
1.4
1.2
1.0
Apparent k_{-3} (s^{-1})
0.00
0.05
0.10
0.15
0.20
Inhibitor concentration, M
mannose

Table 7. Dissociation Rates Observed for Different Immobilization Methods

System	Immobilization Method	Dissociation Rate, s^{-1}
Con A - MUM	CDI	1.8 ± 0.1
	SB	1.8 ± 0.1
Con A - PNPM	CDI	2.6 ± 0.1
	SB	2.6 ± 0.2

two immobilization methods. Possible reasons for this lack of difference is the relative location of the attachment site to the binding site or the number of attachments between protein and support. If the attachment site is removed from the binding site, not only spatially but also in amino acid sequence, any perturbation in the the three-dimensional structure of the protein that might affect the binding of the sugar would be dampened. Increasing the number of bonds between the protein and support would cause greater changes in protein conformation, increasing the probability of changing the kinetic rates.

Since both immobilization methods require amine functionalities in the protein, one might assume that both would affect protein conformation in a similar manner. However, the two methods differ in the kinetic rates observed for immobilized Protein A - IgG complex (14). The lack of variablity in the immobilized Con A - MUM system suggests that each protein will have different changes when they are immobilized. It is likely that no one immobilization method will prove itself to be superior to all others for every protein to be immobilized. Predicting which method would be best for a specific application would depend on a detailed knowledge of the structure of the protein and more knowledge of the reactivity of each reaction method.

Determination of the dissociation rate constant for Con A - OVA complex

The dissociation rate constant of the immobilized Con A - OVA complex was also measured. Both flow rate and inhibitor studies were performed to verify conditions required for the peak decay method. The results are shown

in Figures 17 and 18. While no literature values for this system have been reported, the value $7.2 \pm 0.6 \times 10^{-3}$ s^{-1} is typical of protein - protein interactions (21,22). Muller and Carr have noted that the kinetic rate of the immobilized Con A - OVA complex is much slower than that of immobilized Con A - PNPM complex (33).

Figure 18. Effect of flow-rate on the apparent dissociation rate of the Con A/OVA system with an inhibitor concentration of 1.0 M α-methylmannoside

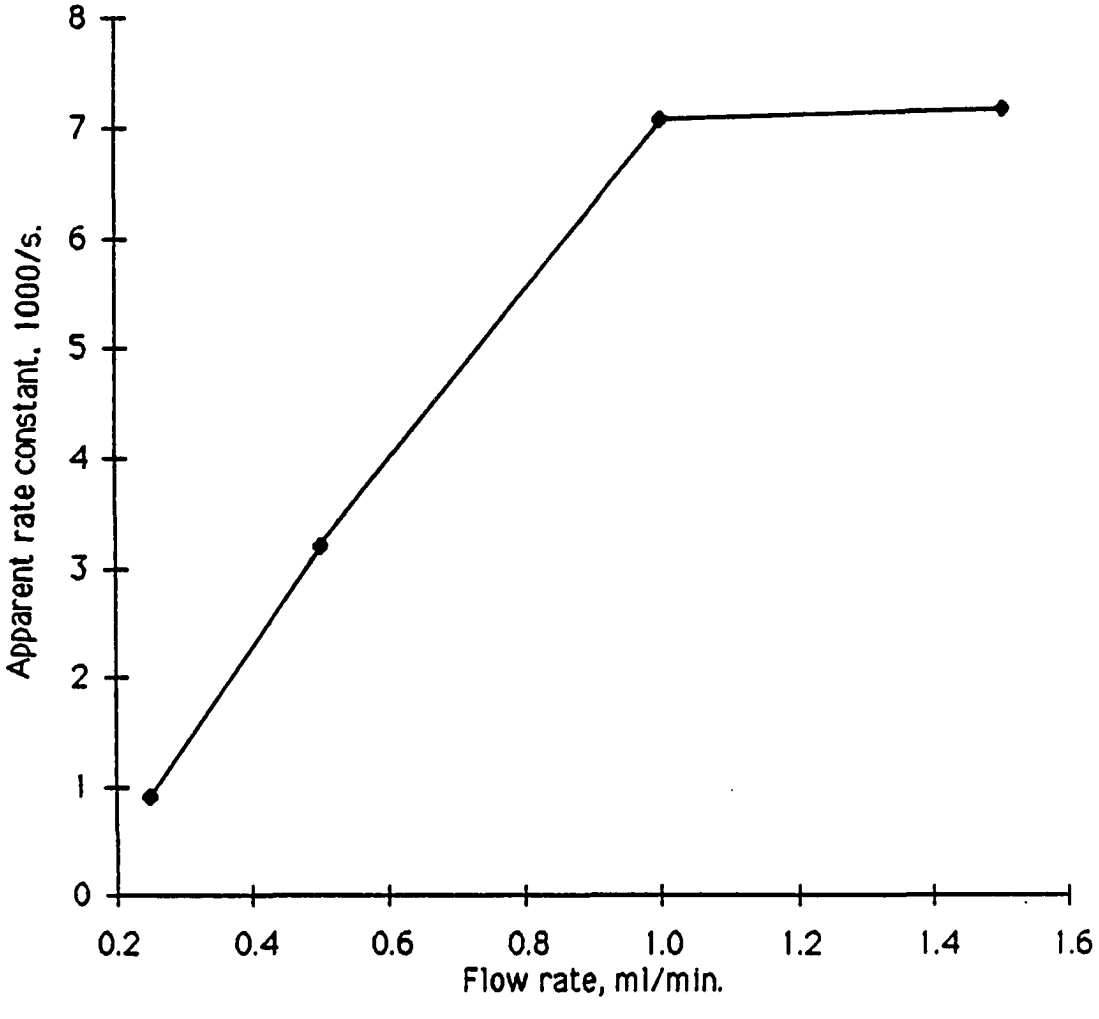
Apparent rate constant, 1000/s.
0
1
2
3
4
5
6
7
8
0.2
0.4
0.6
0.8
1.0
1.2
1.4
1.6
Flow rate, ml/min.

Figure 19. Effect of inhibitor concentration on the apparent dissociation rate constant of the Con A/OVA system at a flow-rate of 1.0 mL/min

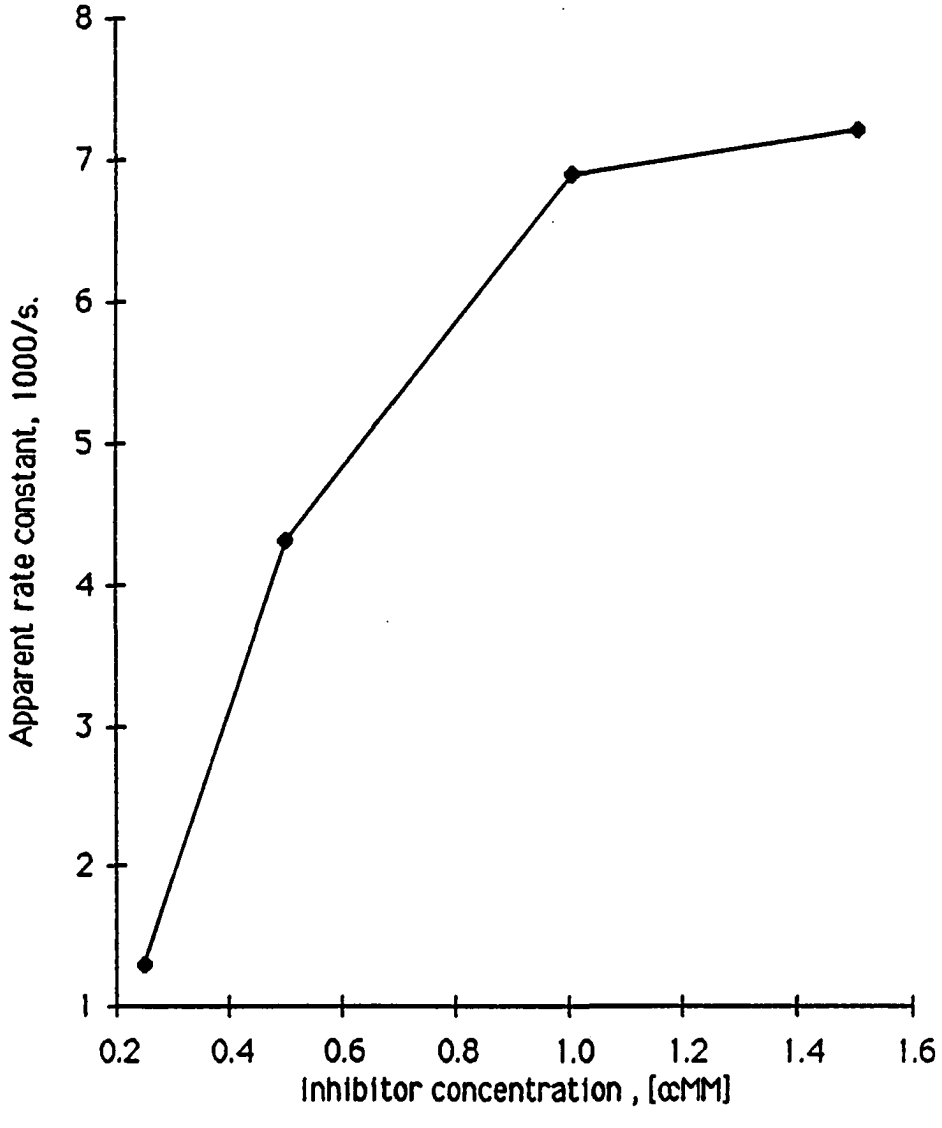
8
7
6
5
4
3
2
1
Apparent rate constant, 1000/s.
0.2
0.4
0.6
0.8
1.0
1.2
1.4
1.6
Inhibitor concentration , [αMM]

SUMMARY

The data presented in this thesis have been based on the application of high-performance affinity chromatography to measure equilibrium and rate constants. The development of these methods has expanded the ability of analysts to examine the interactions of biomolecules that could not have been studied with conventional techniques, such as equilibrium dialysis or ultracentrifugation for the determination of equilibrium constants (34) and stopped-flow or temperature jump methods for kinetic constants (35). The three techniques studied here are representative of how high-performance affinity chromatography can be used (24).

The determination of equilibrium constants has been the best studied application of affinity chromatography. It has advantages over other techniques in the types of complexes that can be studied and in the range of equilibirum constants that can be studied (3). The development of high-performance supports for these measurements has improved their precision and made determination of the thermodynamic parameters feasible. The equilibrium constants determined for immobilized Con A - MUM and immobilized Con A - mannose are in good agreement with those obtained from solution studies. The differences could be the result of uncertainty in the literature values or the result of a systematic error in the HPAC method.

There are several factors that will affect the accuracy of the results. One is the amount of solute injected. Previous work done in our laboratory has demonstrated the importance of maintaining linear elution conditions for

proper measurement (11). The amount of solute injected in these current studies has been selected to fall with the linear isotherm region.

Another possible source of error is the determination of the number of moles of immobilized ligand sites on the column. This quantity was measured with both break-through studies to determine number of active ligand sites and chemical assay to determine the amount of protein immobilized. Both techniques gave the same result, indicating that all of the Con A immobilized was accessible and active.

A final source is the effect of immobilization on the binding of the complex. As discussed earlier, it is quite likely that the immobilization of a macromolecule alters its physicochemical properties. The values obtained for the enthalpies of reaction for the immobilized Con A - MUM interaction falls within the range of values determined for the complex in solution, so that no firm conclusions can be drawn from the equilibrium studies on the effects of immobilization.

The split-peak studies have proved to be inconclusive. The association rate of the Con A - MUM system, with its value of 110,000 $M^{-1}s^{-1}$, probably represent the upper limit of kinetic rates that can be determined by this method. The development of even more efficient packing materials and capillary columns for affinity chromatography and improvements in detection may increase this limit. Alternatively, a system that has a smaller association rate constant could be used to investigate the accuracy of the split-peak method when the binding is reversible during the timescale of the experiment. The studies did support the computer model (11) that has been

used to predict the behavior of the compounds that have been studied. Computer simulations have proved to be a valuable tool in investigating the chromatographic process and in determining what systems could be studied.

The peak-decay experiments have shown themselves to be a precise way to measure the dissociation rates of biomolecular complexes. Since both the peak-decay and isocratic methods utilize competing inhibitors, it is useful to compare the potential advantages of one method over the other.

In the isocratic method, one must generally correct the total plate height for the contributions due to diffusion through the stagnant mobile phase and the eddy diffusion/mobile-phase mass transfer. This involves measurement of linear velocity, pore volume, excluded volume and the diffusion rate constant and recalculation of plate heights as a function of capacity factor, all of which introduce significant uncertainty in the final result (11). In contrast, the rate constant is obtained directly from the slope of the logarithm of the detector response in the peak-decay method.

Some of the calcuation problems of the isocratic method can be avoided if the entire plate height is attributed to kinetic causes. Then only the linear velocity and capacity factor need to be measured. If we consider the case where the ratio of dissociation rate constant to diffusion rate constant is 10 and the pore volume is equal to the excluded volume, it can be shown that, for a capacity factor of 10, the apparent value of the dissociation rate constant would be only 31% of its true value when the contribution by diffusion through the stagnant mobile-phase is not accounted for (15). A more favorable case is when capacity factor is 1, since the kinetic

contributions to band-broadening are at a maximum, while the diffusion term has not yet reached its maximal value. For this set of conditions, the apparent rate constant is still only 69% of its true value. In contrast, for the same system but with capacity factor and void time adjusted in accordance with Equations 35 and 36, the apparent value of the dissociation rate constant would be at least 95% of its true value. Thus, with the peak-decay method, one can measure rate constant accurately when the ratio of dissociation rate constant to diffusion rate constant is greater or equal to 10. With the isocratic method, similar accuracy requires this ratio to be greater or equal to 100.

Other practical advantages of the peak-decay method over the isocratic method include (a) better precision, since slopes rather than variances of the peak profiles are measured, (b) shorter analysis times, since dissociation takes place only once rather than many times, (c) reasonable analysis times, even in cases where the dissociation rate is quite small, and (d) improved detectability, because the column can be saturated with solute.

Potentially offsetting these advantages are the need to use very high inhibitor concentrations to reduce the capacity factor, and high flow-rates and/or small columns to minimize the void time in cases where the dissociation rate constant is moderately large. Since there is a step change in mobile phase at time zero, detectability may be adversely affected by refractive-index effects.

A comparison of the peak-decay method and the isocratic method (11) for the determination of the dissociation rate of immobilized Con A - MUM and

Con A - PNPM systems indicate that the peak-decay method does indeed have advantages over the isocratic method. Precision for the peak-decay method was 5.6% RSD compared to 30% RSD for the isocratic method. Analysis time was reduced to 10 minutes. The constraints on column size, flow-rate and inhibitor concentration were not major impedements for the experiments.

Preliminary calculations taking into account analysis time, inhibitor concentration, flow-rate, column size and detectability in Reference 35 may be useful in determining whether isocratic or peak-decay experiments are feasible in particular situations. Since there were some discrepancies between the model used to obtain Equations 31-36 and the experimental data, particularly in the case of flow-rate effects, it is suggested that Equations 31-36 be used only to establish initial conditions for peak-decay measurements. Flow-rate and inhibitor concentration studies should be performed to ensure that the "plateau" value of the dissociation rate has been reached.

While only competitive inhibitors were used in these studies, the peak-decay method also is appropriate for the kinetic evaluation of non-specific elution methods. If both acidic solutions and organic solvents denature a particular affinity ligand-solute complex, it would be of fundamental and practical interest to determine the apparent dissociation rate constant for each eluent and to compare each with the value obtained from competitive elution.

The differences between the dissociation rates for the solution and the immobilized values provide the strongest indication that there is some

difference between the physicochemical properties of the protein when in solution and when immobilized. As discussed earlier, it is difficult to generalize until much more is known about the reactivity of the various methods of immobilization and the factors that maintain the tertiary structure of the protein. With the ability to measure the equilibrium and kinetic constants as discussed in this thesis, analysts are now in the position to study how these parameters are affected by different immobilization methods.

BIBLIOGRAPHY

1. Andrews, P.; Kitchen, B. J.; Winzor, D. J. Biochem. J. 1973, 135, 897.

2. Dunn, B. M.; Chaiken, I. M. Proc. Nat. Acad. Sci. USA 1974, 71, 2382.

3. Chaiken, I. M. Anal. Biochem. 1979, 97, 1.

4. Dunn, B. M. Applied Biochem. Biotechnol. 1984, 9, 261.

5. Denizot, F. C.; Delaage, M. A. Proc. Nat. Acad. Sci. USA 1975, 72, 4840.

6. Long, R. H.; Chaiken, I. M. unpublished data cited in reference 3.

7. Katoh, S.; Kambayashi, T.; Deguch, R.; Yoshida, F. Biotechnol. Bioengin. 1978, 20, 267.

8. Kasche, V.; Buchholz, K.; Galunsky, B. J. Chromatogr. 1981, 216, 169.

9. Nilsson, K.; Larsson, P.-O. Anal. Biochem. 1983, 134, 60.

10. Muller, A. J.; Carr, P. W. J. Chromatogr. 1984, 284, 33.

11. Anderson, D. J.; Walters, R. R. J. Chromatogr. 1986, 376, 69.

12. Chase, H. A. J. Chromatogr. 1984, 297, 179.

13. Sportsman, J. R.; Liddil, J. D.; Wilson, G. S. Anal. Chem. 1983, 55, 771.

14. Hage, D. S.; Walters, R. R.; Hethcote, H. W. Anal. Chem. 1986, 58, 274

15. Moore, R. M.; Walters, R. R. J. Chromatogr. 1987, 384, 91.

16. Eilat, D.; Chaiken, I. M. Biochemistry 1979, 18, 790.

17. Hethcote, H. W.; DeLisi, C. J. J. Chromatogr. 1982, 248, 183.

18. Giddings, J.C.; Eyring, H. J. Phys. Chem. 1955, 59, 416.

19. Espenson, J.H. "Chemical Kinetics and Reaction Mechanisms" McGraw-Hill, New York, 1981, p. 65.

20. Rakowski, A. Z. Phys. Chem. 1906, 57, 321.

21. Karger, B.L.; Snyder, L.R.; Horvath, C. "An Introduction to Separation Science" John Wiley and Sons, New York, 1973, p. 110.

22. Cunningham, B.A.; Wang, J.L.; Pflumm, M.N.; Edelman, G.M. Biochemistry 1972, 11, 3233.

23. Walters, R.R. Anal. Chem. 1982, 54, 591.

24. Walters, R.R. in Dean, P.D.G.; Johnson, W.S.; Middle, F.A., Eds. "Affinity Chromatography: A Practical Approach", IRL Press, Oxford, 1985, p. 25.

25. Larsson, P.-O.; Glad, M.; Hansson, L.; Mansson, M.-O.; Ohlson, S. Mosbach, K. Adv. Chromatogr. 1983, 21, 41.

26. Crowley, S.C.; Chan, K.C.; Walters, R.R. J. Chromatogr. 1986, 359, 359.

27. Guggenheim, E.A. Philos. Mag. 1926, 2, 538.

28. Loontiens, F.G.; Clegg, R.M.; Jovin, T.M. Biochemistry, 1977, 16, 159.

29. Clegg, R.M.; Loonteins, F.G.; Jovin, T.M. Biochemistry, 1977, 16, 197.

30. Moore, W.S. "Physical Chemistry", Prentice-Hall, Englewood Cliffs, New Jersey, 1972, p. 363.

31. Clegg, R.M.; Loontiens, F.G.; Van Landschoot, A; Jovin, T.M. Biochemistry, 1981, 20, 4687.

32. Muller, A.J.; Carr, P.W. J. Chromatogr., 1984, 294, 235.

33. Steinnardt, J.; Reynolds, J.A. "Multiple Equilibria in Proteins"; Academic Press: New York, 1969; Chapter 3.

34 Dunford, H.B. In "Fast methods in Physical Biochemistry and Cell Biology"; Sha'afi, R.I.; Fernandez, S.M., Editors; Elsevier Science Publishers: Amsterdam, 1983; Chapter 2.

ACKNOWLEDGEMENT

I wish to express my sincere appreciation to Dr. Rod Walters for his advice, assistance and patience during my graduate studies. Working for Dr. Walters has taught me much more than just analytical techniques and I feel grateful for what I have learned from him.

I have always believed that it is the people that you spend time with that makes whatever you are doing worthwhile and that has certainly been true in graduate school. I would like to thank Pearl, Peggy, Verla, Max, Ray and Bill from Chem Stores; Eldon, John and George from the shop; Harvey, Dr. Deihl and Dr. Johnson from Chem 211; my fellow classmates; and especially the other members of the research group: Dave Anderson, Sam and Melissa Crowley, John Graham, Dave and Jill Hage, Danlin and Jean Wu, Larry Larew, Jackie and Ashley Annalt and King Chan. In the future, let it be said that for a brief, shining moment there was the Walters' Research Group.

Finally, I would like the offer my deepest thanks to my wife, Sheryl, and son, Robbie. They have endured my ups and downs and given me the love and support that I needed throughout my graduate studies. Whatever had happened in the laboratory that day, I knew they would be there to lift my spirits, ease my disappointments and share my joy. Thank you seems inadequate, so let me say to them "I love you".